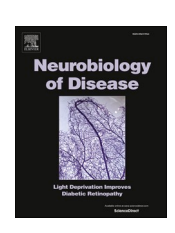
ELSEVIER

Contents lists available at ScienceDirect

Neurobiology of Disease

journal homepage: www.elsevier.com/locate/ynbdi



ATXN2L primarily interacts with NUFIP2, the absence of ATXN2L results in NUFIP2 depletion, and the ATXN2-polyQ expansion triggers NUFIP2 accumulation

Jana Key^{a,1}, Luis-Enrique Almaguer-Mederos^{a,1}, Arvind Reddy Kandi^a, Nesli-Ece Sen^a, Suzana Gispert^a, Gabriele Köpf^a, David Meierhofer^b, Georg Auburger^{a,c,*}

ARTICLE INFO

Keywords: interactome profiling stress granules Spinocerebellar Ataxia actin cytoskeleton proteome profiling RNA-binding proteins ribonucleoprotein complexes

ABSTRACT

The cytoplasmic Ataxin-2 (ATXN2) protein associates with TDP-43 in stress granules (SG) where RNA quality control occurs. Mutations in this pathway underlie Spinocerebellar Ataxia type 2 (SCA2) and Amyotrophic Lateral Sclerosis. In contrast, Ataxin-2-like (ATXN2L) is predominantly perinuclear, more abundant, and essential for embryonic life. Its sequestration into ATXN2 aggregates may contribute to disease. In this study, we utilized two approaches to clarify the roles of ATXN2L. First, we identified interactors through co-immunoprecipitation in both wild-type and ATXN2L-null murine embryonic fibroblasts. Second, we assessed the proteome profile effects using mass spectrometry in these cells. Additionally, we examined the accumulation of ATXN2L interactors in the SCA2 mouse model, Atxn2-CAG100-KnockIn (KIN). We observed that RNA-binding proteins, including PABPN1, NUFIP2, MCRIP2, RBMS1, LARP1, PTBP1, FMR1, RPS20, FUBP3, MBNL2, ZMAT3, SFPQ, CSDE1, HNRNPK, and HNRNPDL, exhibit a stronger association with ATXN2L compared to established interactors like ATXN2, PABPC1, LSM12, and G3BP2. Additionally, ATXN2L interacted with components of the actin complex, such as SYNE2, LMOD1, ACTA2, FYB, and GOLGA3. We noted that oxidative stress increased HNRNPK but decreased SYNE2 association, which likely reflects the relocalization of SG. Proteome profiling revealed that NUFIP2 and SYNE2 are depleted in ATXN2L-null fibroblasts. Furthermore, NUFIP2 homodimers and SYNE1 accumulate during the ATXN2 aggregation process in KIN 14-month-old spinal cord tissues. The functions of ATXN2L and its interactors are therefore critical in RNA granule trafficking and surveillance, particularly for the maintenance of differentiated neurons.

1. Introduction

The quality control of ribonucleoprotein (RNP) granules during long-distance transport in neurites is crucial for the stimulus-dependent mRNA translation in synapses (Linder et al., 2015; Sahoo et al., 2018; Moon et al., 2020; Elaswad et al., 2022; Dhaliwal et al., 2022). Impairments in this pathway cause neurodegeneration preferentially of motor neurons and cerebellar neurons (Lefebvre et al., 1995; Neumann et al., 2006; Kwiatkowski Jr et al., 2009; Elden et al., 2010; Guerrero et al., 2016; Singh et al., 2017; Becker et al., 2017; Klockgether et al.,

2019; Mandrioli et al., 2020). When cellular growth periods are interrupted by significant damage, the RNP granules coalesce into cytosolic stress granules (SG) where surveillance mechanisms decide to repair individual RNAs or degrade them in P-bodies (Youn et al., 2019; Corbet and Parker, 2019; Riggs et al., 2020). The trafficking and surveillance machinery controls association with or dissociation from mRNAs at adenine-enriched sequences, known as poly(A) stretches (Passmore and Coller, 2022), or at uracil-enriched sequences, known as AU-rich elements (ARE) (Chen and Shyu, 1995). It also controls the RNA winding into double-strand (ds)-hairpins or their unwinding via helicases

a Goethe University Frankfurt, University Hospital, Clinic of Neurology, Experimental Neurology, Heinrich- Hoffmann-Str. 7, 60528 Frankfurt am Main, Germany

b Max Planck Institute for Molecular Genetics, Ihnestraße 63-73, 14195 Berlin, Germany

^c Institute for Clinical Neuroanatomy, Dr. Senckenberg Anatomy, Fachbereich Medizin, Goethe University Frankfurt, Frankfurt am Main, Germany

^{*} Corresponding author at: Goethe University Frankfurt, University Hospital, Clinic of Neurology, Experimental Neurology, Heinrich- Hoffmann-Str. 7, 60528 Frankfurt am Main, Germany.

E-mail address: auburger@em.uni-frankfurt.de (G. Auburger).

joint first authorship

(Hardwick and Luisi, 2013), assesses the RNA posttranscriptional modifications (Roundtree et al., 2017), and liquid-liquid phase separation (Krainer et al., 2021).

As a prime member of this SG surveillance machinery (Nonhoff et al., 2007; Swisher and Parker, 2010; Kaehler et al., 2012; Seidel et al., 2017a), Ataxin-2 contains a Like-Sm (LSm) domain together with an LSm associated domain (LSm-AD) sequence to interact with helicases such as DDX6 (Nonhoff et al., 2007; Kaehler et al., 2012; Lee et al., 2017a; Inagaki et al., 2021; Wang et al., 2024) and to bind singlestranded (ss) ARE (Yokoshi et al., 2014; Singh et al., 2021). Furthermore, it contains a PAM2 motif to associate with ss-poly(A) stretches indirectly via poly(A)-binding-proteins (Albrecht and Lengauer, 2004; Ralser et al., 2005a; Satterfield and Pallanck, 2006; Kozlov et al., 2010; Damrath et al., 2012; Jimenez-Lopez and Guzman, 2014). These motifs enable not only surveillance of mRNAs, but also effects on rRNA, microRNA and long-noncoding RNA effects have been documented (McCann et al., 2011; Sudhakaran et al., 2014; Salvi et al., 2014; Li et al., 2021; Paul et al., 2024). This characteristic combination of sequence motifs is first detected in eukaryotic organisms, such as in the yeast ortholog PBP1 (Mangus et al., 1998; Mangus et al., 2004; Kimura et al., 2013), and exists as a single copy in nematodes such as Caenorhabditis elegans ATX-2 (Kiehl et al., 2000; Ciosk et al., 2004; Maine et al., 2004; Bar et al., 2016; Stubenvoll et al., 2016a), or flies such as Drosophila melanogaster dATX2 (Satterfield et al., 2002; Al-Ramahi et al., 2007; Vianna et al., 2016). In contrast, land plants contain two gene copies named CID3 versus CID4 (Jimenez-Lopez and Guzman, 2014; Bravo et al., 2005; Lopez-Juarez et al., 2021), while mammals also contain two gene copies known as the less abundant ATXN2 versus the more abundant ATXN2L, with complementary roles for translation oscillations and SG (Ayache et al., 2015; Zhuang et al., 2023). Under unstressed growth conditions, Ataxin-2 isoforms are localized with the translation apparatus at the endoplasmic reticulum (Satterfield and Pallanck, 2006; Lastres-Becker et al., 2008a; van de Loo et al., 2009; Fittschen et al., 2015; Lastres-Becker et al., 2016; Del Castillo et al., 2019; Inagaki et al., 2020) and with microtubules (Gnazzo et al., 2016; Stubenvoll et al., 2016b; Del Castillo et al., 2022; Boeynaems et al., 2023).

ATXN2 was first described, because pathogenic expansions of an Nterminal polyglutamine (polyQ) stretch from the normal length Q22/ Q23 beyond a size of Q33 cause the autosomal dominantly inherited, neurodegenerative disorder Spinocerebellar Ataxia type 2 (SCA2) (Trottier et al., 1995; Pulst et al., 1996; Imbert et al., 1996; Sanpei et al., 1996), where the glutamatergic corticospinal motor neurons and the glutamatergic cerebellar granular neuron projections to Purkinje cells are preferentially affected (Estrada et al., 1999; Lastres-Becker et al., 2008b; Rub et al., 2013; Velazquez-Perez et al., 2016; Seidel et al., 2017b; Velazquez-Perez et al., 2017a; Velazquez-Perez et al., 2017b; Velazquez-Perez et al., 2018; Ruiz-Gonzalez et al., 2020; Glass et al., 2022). Much more infrequently, a Parkinson's disease phenotype is triggered by the same monogenic polyQ expansions due to early loss of dopaminergic midbrain neurons (Lu et al., 2002; Charles et al., 2007; Schols et al., 2015; Nkiliza et al., 2016; Kim et al., 2017; Miyaue et al., 2017; Casse et al., 2023). ATXN2 polyQ expansions of intermediate size between Q27 and Q33 act as polygenic modifiers that exacerbate the progression of the adult motor neuron diseases Amyotrophic Lateral Sclerosis (ALS) and Fronto-Temporal Lobar Dementia (FTLD) (Elden et al., 2010; Lee et al., 2011; Yu et al., 2011; Gispert et al., 2012; Van Langenhove et al., 2012; Baumer et al., 2014; van Blitterswijk et al., 2014; Li et al., 2016; Borrego-Hernandez et al., 2024), and of Parkinson syndrome (Parkinson plus) (Ross et al., 2011; Sen et al., 2016). Conversely, the knockout (KO) or knockdown (KD) of ATXN2 was shown to strongly mitigate the progression of such diseases (Becker et al., 2017; Scoles et al., 2017; Auburger et al., 2017), and this makes ATXN2 a prime pharmacological target for the prevention of neurodegenerative processes that are triggered by RNA toxicity (van den Heuvel et al., 2014; Scoles and Pulst, 2018; Amado and Davidson, 2021; Scoles et al., 2022).

Although ATXN2L is the more abundant and more important paralog in cellular life, and although it may play a compensatory role for ATXN2 mutations (Felicio et al., 2023), only a few studies have focused on it so far. Mice with homozygous deletions of Atxn2l exons 5-8, which results in the production of an N-terminal fragment but absence of the LSm, LSm-AD and PAM2 domains until the C-terminus, show mid-embryonic lethality with brain cortex lamination defects, while the heterozygous mutants appeared normal (Key et al., 2020). In comparison, the less abundant ATXN2 paralog would appear barely relevant, since mice with homozygous deletions of Atxn2 exon1, which results in the production of a minimal N-terminal fragment but absence of the LSm, LSm-AD and PAM2 domains until the C-terminus, show only age-associated obesity, hepatosteatosis, insulin resistance and dyslipidemia, with reduced fertility and locomotor hyperactivity (Lastres-Becker et al., 2008a; Fittschen et al., 2015; Lastres-Becker et al., 2016; Kiehl et al., 2006; Meierhofer et al., 2016). ATXN2L and ATXN2 expression is conversely modulated by growth factor signaling versus stress conditions (Lastres-Becker et al., 2016; Key et al., 2020; Lin et al., 2019). Unlike ATXN2, the human promoter for ATXN2L expression is shown to change conformation upon exposition to G-quadruplex ligands (Abdelhamid et al., 2019). Again unlike ATXN2, the human transcript for ATXN2L contains a SINE-VNTR-Alu element, which could modulate exon extension or alternative transcript regulation by stress events (Kwon et al., 2013). An intron in the ATXN2L pre-mRNA gives rise to a lariat-derived circRNA (Robic et al., 2020; Robic et al., 2022). All these observations suggest that human cells have developed multiple mechanisms to fine-tune the expression of ATXN2L in dependence on diverse feedbacks, as a highly relevant molecule. While both, ATXN2L and ATXN2, are found among the >300 RNA-binding proteins (RBPs) in the stress granule proteome (Ayache et al., 2015; Markmiller et al., 2018; Marmor-Kollet et al., 2020; Freibaum et al., 2021), it is unclear so far, with which factors they have close interaction and share functional cooperation. In the human cervical cancer cell line HeLa, preferential interactions within SG were reported between ATXN2L, ATXN2, DDX1, FAM98A, and NUFIP2 (Ozeki et al., 2019). Indeed, the relocalization of ATXN2L to SG depends on PRMT1-mediated arginine methylation (Kaehler et al., 2015), and FAM98A and DDX1 are activators of this post-translational modification (Akter et al., 2017), so FAM98A and DDX1 seem to be upstream factors that determine the trafficking changes of specific ribonucleoproteins (RNPs) during the switch from growth to stress periods. The role of the polysome-associated factor and DDX6 interactor NUFIP2 (Bardoni et al., 2003; Bish et al., 2015) in this SG subcomplex remains unclear. Another preferential interaction for ATXN2L was claimed with the RNA-binding, cold shock domain-containing protein YBX1 (Tang et al., 2024; Mordovkina et al., 2020). Variants in the human ATXN2L gene have been reported in very few live patients so far (Alzahrani et al., 2021; Kaplanis et al., 2020), who showed developmental delay and macrocephaly.

Here, we performed (i) coimmunoprecipitation and mass spectrometry analyses in WT and ATXN2L-null mouse embryonic fibroblasts (MEF), (ii) global proteome profiling via label-free mass spectrometry in wildtype (WT) and ATXN2L-null MEF, (iii) the analysis of ATXN2L interactor proteins in 14-month-old spinal cords from mice with progressive ATXN2 aggregation due to the *Atxn2*-CAG100-KnockIn (KIN) mutation as established SCA2 model (Damrath et al., 2012; Halbach et al., 2015; Halbach et al., 2017; Sen et al., 2019a; Sen et al., 2019b; Arsovic et al., 2020; Canet-Pons et al., 2021; Bux et al., 2023). With this strategy, we aimed to identify protein interactors that depend on ATXN2L in their abundance, and undergo changes during the motor neurodegeneration process in SCA2 models. Our work elucidates the pathways that are important for the survival of differentiated neurons under stress.

2. Materials and methods

2.1. MEF culture, treatment, coimmunoprecipitation, and proteome profiling

The generation and culture of 5 WT and 5 ATXN2L-null MEF lines was done as previously reported (Key et al., 2020). For that, at gestational day 14 of heterozygous breeder mice, the embryos were taken out and the skin of the embryos was dissected, homogenized, and trypsinized for 10 min at 37 °C. The cells were cultured in DMEM, containing 4.5 g/L D-glucose, 1% L-glutamine, 1% Penicillin/Streptomycin and 10% FCS, and DNA was extracted for genotyping. Their exposure to sodium arsenite (NaARS) stress also followed published protocols (Sen et al., 2019b). In these experiments, the cells were plated in 175 cm² flasks and allowed to grow until they reached about 90% confluence before being treated with 0.5 mM NaARS (Sigma Aldrich, St. Louis, MO, USA, #S7400) for 45 minutes. Then, MEFs were ruptured in a lysis buffer - 20 mM Tris/HCl pH 8.0, 137 mM NaCl, 2 mM EDTA, 1% NP40, 1% glycerol with Protease-Inhibitor Cocktail cOmplete (Roche Diagnostics, Mannheim, Germany) - via 30 min head-to-head rotation at 4 °C. Nuclear debris was removed via centrifugation at full speed at 4 °C for 20 min. The protein content was determined via BCA (Life Technologies, Karlsruhe, Germany). A total of 1000 µg of protein lysate was incubated with 4 µg of pull antibody (anti-ATXN2L from Invitrogen, Carlsbad, CA, USA #PA5-59601, or normal rabbit IgG from Cell Signaling Technology, Danvers, MA, USA #2729) and rotated for 2 h at room temperature (RT). In the meantime, 1.5 mg of Dynabeads (Thermo Fisher, #10004D) was washed 3 times with PBS/T and added to the lysate/antibody solution. The mix was rotated head-to-head for 60 min at RT, to be either analyzed by immunoblot as described in the following sentences, or by nano LC-MS/MS as described in the subsequent paragraph. For immunoblots, 5 washes with PBS were performed, then the tubes were fixed on a magnetic stand and elution was carried out with 40 μL of 50 mM glycine, pH 2.8. The eluate was mixed with a loading buffer, boiled for 5 min at 90 $^{\circ}$ C, and loaded for SDS electrophoresis. The antibodies used for co-IP detection were ATXN2L (Proteintech, Rosemont, IL, USA, #24822-1-AP) or PABP (Abcam, Cambridge, UK, #ab21060).

2.2. "On beads" digest for Co-IP samples

Four MEF coimmunoprecipitation samples on magnetic beads (Thermo Scientific Pierce, Waltham, MA, MS-Compatible Magnetic IP Kits, catalogue no: 90409) were washed 3 times in 100 mM ammonium bicarbonate buffer. This was followed by tryptic digestion including reduction and alkylation of cysteines. Reduction was performed by adding tris(2-carboxyethyl)phosphine to a final concentration of 5.5 mM at 37 °C on a rocking platform (600 rpm) for 30 min in a total volume of 150 µL. For alkylation, chloroacetamide was added to a final concentration of 24 mM at room temperature on a rocking platform (600 rpm) for 30 min. Proteins were then digested with 100 ng trypsin (Roche, Basel, Switzerland) per sample at pH 8, shaken at 800 rpm at 37 °C for 18 h. The samples were acidified by adding 3.75 μL of 100% formic acid (2% final concentration), centrifuged briefly and placed on the magnetic rack. The supernatants containing the digested peptides were transferred to a new low-protein binding tube. Peptide desalting was performed on self-packed C18 columns in a tip. Eluates were lyophilized and reconstituted in 38 μL of 5% acetonitrile and 2% formic acid in water, briefly vortexed and sonicated in a water bath for 30 sec before injecting 20 µL onto a nano-LC-MS/MS.

2.3. Global proteomics

10 MEF samples (5 Atxn2l KO and 5 WT) were lysed under denaturing conditions in 300 μ l of a buffer containing 3 M guanidinium chloride (GdmCl), 10 mM tris(2-carboxyethyl)phosphine, 40 mM

chloroacetamide, and 100 mM Tris-HCl pH 8.5. Lysates were denatured at 95°C for 10 min shaking at 1000 rpm in a thermal shaker and sonicated in a water bath for 10 min. The protein concentration of each sample was measured with a BCA protein assay kit (23252, Thermo Scientific, USA). 30 µg of each sample was diluted with a dilution buffer containing 10% acetonitrile and 25 mM Tris-HCl, pH 8.0, to reach a 1 M GdmCl concentration. Then, proteins were digested with LysC (Roche, Basel, Switzerland; enzyme to protein ratio 1:50, MS-grade) shaking at 700 rpm at 37°C for 2 hours. The digestion mixture was diluted again with the same dilution buffer to reach 0.5 M GdmCl, followed by tryptic digestion (Roche, enzyme to protein ratio 1:50, MS-grade) and incubation at 37°C overnight in a thermal shaker at 700 rpm. Peptide desalting was performed according to the manufacturer's instructions (Pierce C18 Tips, Thermo Scientific, Waltham, MA). Desalted peptides were reconstituted in 0.1% formic acid in water and further separated into four fractions by strong cation exchange chromatography (SCX, 3M Purification, Meriden, CT). Eluates were first dried in a SpeedVac, then dissolved in 5% acetonitrile and 2% formic acid in water, briefly vortexed, and sonicated in a water bath for 30 seconds prior injection to nano-LC-MS/MS.

2.4. LC-MS/MS instrument settings for shotgun proteome profiling and data analysis

Liquid chromatography-tandem mass spectrometry (LC-MS/MS) was performed using nanoflow reversed-phase liquid chromatography (Dionex Ultimate 3000, Thermo Scientific) coupled online to a Q-Exactive HF Orbitrap mass spectrometer (Thermo Scientific), as previously reported (Gielisch and Meierhofer, 2015). Briefly, LC separation was performed using a PicoFrit analytical column (75 μm ID \times 50 cm long, 15 µm tip ID; New Objectives, Woburn, MA) packed in-house with 3 μm C18 resin (Reprosil-AQ Pur, Dr Maisch, Ammerbuch, Germany). Peptides were eluted using a gradient of 3.8 to 38% solvent B in solvent A over 120 min at a flow rate of 266 nL per minute. Solvent A was 0.1% formic acid and solvent B was 79.9% acetonitrile, 20% H₂O and 0.1% formic acid. The nanoelectrospray was generated by applying 3.5 kV. A cycle of one full Fourier transform scan mass spectrum (300-1750 m/z, resolution of 60,000 at m/z 200, automatic gain control (AGC) target 1 imes 106) was followed by 12 data-dependent MS/MS scans (resolution of 30,000, AGC target 5 \times 105) with a normalized collision energy of 25 eV. A dynamic exclusion window of 30 sec was used to avoid multiple sequencing of the same peptides.

Raw MS data were processed using MaxQuant software (v2.2.0.0) and searched against the Mus musculus proteome database UniProtKB UP000000589 with 55,260 protein entries, released in June 2023. MaxQuant database search parameters were a false discovery rate (FDR) of 0.01 for proteins and peptides, a minimum peptide length of seven amino acids, a first search mass tolerance for peptides of 20 ppm, and a main search tolerance of 4.5 ppm. A maximum of two missed cleavages was allowed for tryptic digestion. Cysteine carbamidomethylation was set as a fixed modification, while N-terminal acetylation and methionine oxidation were set as variable modifications. The MaxQuant processed output files can be found in Supplementary Table 1, showing peptide and protein identification, accession numbers, % sequence coverage of the protein and q values. The mass spectrometry data have been deposited at the ProteomeXchange Consortium (http://proteomecent ral.proteomexchange.org) via the PRIDE partner repository (Martens et al., 2005) with the data set identifier PXD061048 for MEF proteome profiles, and PXD061161 for MEF Co-IPs.

2.5. Fluorescent immunocytochemistry

The microscopic detection of ATXN2L or ATXN2 compared with NUFIP2 in MEF cultures, without versus with NaARS-mediated oxidative stress to validate their co-localization in stress granules, was performed as previously described (Sen et al., 2019b). In brief, 5×10^4 cells

from WT and ATXN2L-null (KO) MEF cultures were seeded on 12 mm cover slips and cultured over night. The cells were washed and stressed with 0.5 mM NaARS, supplemented in the DMEM growth medium for 45 min at 37 °C. Control cells were washed and supplemented with only DMEM growth medium for 45 min. Cells were washed once before fixation with 4% paraformaldehyde/PBS at room temperature (RT) for 20 min, and then permeabilized with 0.1% Triton-X-100/PBS for 20 min at RT. Blocking was conducted with a 3% BSA/PBS solution for 1 h at RT. The primary antibody incubation was performed in 3% BSA/PBS for 1 h at RT, using the following antibodies: ATXN2L (Proteintech, #24822-1-AP) with NUFIP2 (Proteintech, #67195-1-Ig), ATXN2 (BD Transduction, #611378) with NUFIP2 (Proteintech, 17752-1-AP). The secondary antibody was performed in 3% BSA/PBS for 1 h at RT in the dark. The coverslips were mounted on glass slides with fluorescent mounting medium (Thermo Fisher) and dried overnight. Cell imaging was performed using Zeiss Axiovert 200 M inverted microscope or confocal microscope Keyence, BZ-X series, and ImageJ software was used to merge images. Triple immunofluorescence quantification was done using ImageJ (v2.14.0/1.54p). A direct line through the center of the nucleus was straightened with 20 pixel width. Plot profiles from the entire area were normalized to average intensity for each channel separately. Graphs were generated with GraphPad Prism 10.

2.6. Breeding, aging, genotyping, and dissection of Atxn2-CAG100-KnockIn mice

Spinal cord tissues from 14-month-old mice were obtained as previously described (Sen et al., 2019b; Canet-Pons et al., 2021) and stored at -80 °C until analysis. The study was ethically assessed by the Regierungspraesidium Darmstadt, with approval number V54-19c20/ 15-FK/1083. In detail, animals were housed at the Central Animal Facility (ZFE) of the Goethe University Medical School, Frankfurt am Main. They were kept in individually ventilated cages at a 12 h-light/12 h-dark cycle under routine health monitoring and fed ad libitum. During aging, mice were monitored regularly for health issues, with food and liquid being supplied at the cage bottom to ensure sufficient nutrition despite locomotor restrictions. Mice were killed by decapitation or cervical dislocation and the spinal chords were dissected. To confirm correct genotype, DNA was isolated from ear punches and the genotyping PCR was performed. TaKaRa LA Taq-Polymerase (Takara Bio Inc., Japan) was used to amplify the neomycin cassette excised locus with the primer pair NOW1-K2 5'-TGAGTTGACTCCACAGGGAGGTGAGC-3' and NOW1-H2 5'-CCATCTCGCCAGCCCGTAAGATTC-3' flanking this site. The conditions were: initial denaturation at 94 °C for 3', followed by 30 cycles of denaturation at 94 °C for 15", annealing at 68 °C for 4', elongation at 68 °C for 4', and a final elongation step at 68 °C for 9'. The wild-type (WT) allele is predicted to yield an amplification product of 793 bp, while the CAG100 allele yields 948 bp.

2.7. Spinal cord protein extraction and quantitative immunoblotting

Mouse cervicothoracic spinal cord tissues from a total of 10 mice (5 mutant and 5 WT) were homogenized with a motor pestle in 5-10x weight/volume amount of RIPA buffer consisting of 50 mM Tris-HCl (pH 8.0), 150 mM NaCl, 2 mM EDTA, 1% Igepal CA-630 (Sigma Aldrich, St. Louis, MO), 0.5% sodium deoxycholate, 0.1% SDS, cOmpleteTM Protease Inhibitor Cocktail (Roche), and HaltTM Phosphatase Inhibitor Cocktail (Thermo Fisher Scientific). Similarly, MEF and human skin fibroblast pellets were homogenized in RIPA buffer by pipetting. The resulting protein suspensions were sonicated, and protein concentration was determined in a Tecan Spark plate reader (Tecan Group Ltd, Männedorf, Switzerland) using a PierceTM BCA protein assay kit (Thermo Fisher Scientific). 15 to 25 µg of total proteins were mixed with 6x loading buffer consisting of 250 mM Tris-HCl pH7.4, 20% glycerol, 4% SDS, 10% 2-mercaptoethanol, and 0.005% bromophenol blue, incubated at 90 °C for 5 min, separated on 8-15% polyacrylamide gels at

120 Volts, and transferred to nitrocellulose membranes (0.2 µm) (Bio-Rad Laboratories, Hercules, CA). The nitrocellulose membranes were blocked in 5% BSA/TBS-T, and incubated overnight at 4 °C with primary antibodies. Afterwards, the nitrocellulose membranes were incubated for 1 h at room temperature, with fluorescently labeled secondary IRDye® 800CW goat anti-mouse (LI-COR 926-32210, 1:10,000), IRDye® 800CW goat anti-rabbit (LI-COR 926-32211, 1:10,000), IRDye® 680RD goat anti-mouse (LI-COR 926-68070, 1:10,000) or IRDve® 680RD goat anti-rabbit (LI-COR 926-68071, 1:10,000). Membranes were scanned using an Odyssey® Classic Imager. Image visualization and quantification of signal intensities were performed using Image StudioTM software (version 5.2) (LI-COR Biosciences, Lincoln, NE). The following primary antibodies were used: ATXN2L (Proteintech, Rosemont, IL, USA, #24822-1-AP), ATXN2 (Proteintech, #21776-1-AP), NUFIP2 (Proteintech, #17752-1-AP), NUFIP1 (Proteintech, #12515-1-AP), SYNE2 (Invitrogen, #PA5-78438) and DCLK1 (Cell Signaling Technology, #62257). GAPDH (Calbiochem, San Diego, CA, USA, #CB1001, 1:10000) served as loading controls. Precision Plus Protein™ All Blue Prestained Protein Standards (Bio-Rad, Hercules, CA, USA, #1610373) was used as size marker.

2.8. Reverse transcriptase quantitative real-time polymerase chain reaction (RT-qPCR)

Total RNA isolation from aged spinal cord tissue and MEF pellets was performed with TRIzol Reagent (Sigma Aldrich) according to manufacturer's instructions. Total RNA yield and purity were quantified using a Tecan Spark plate reader at 230, 260, and 280 nm, in a NanoQuant plate. cDNA synthesis was performed from 1 µg of total RNA template using the SuperScript IV VILO kit (Invitrogen) according to the manufacturer's instructions. Gene expression profiles were assessed by RTqPCR using a StepOnePlusTM (96 well) Real-Time PCR System (Applied Biosystems, Foster City, CA, USA). RT-qPCRs were run in technical duplicates on cDNA from 25 ng total RNA, with 1 µl TaqMan® Assay, 10 µl FastStart Universal Probe Master 2× (Rox) Mix (Roche) and ddH2O up to 20 μ l of total volume. The PCR cycling conditions were 50 $^{\circ}$ C for 2 min, 95 $^{\circ}$ C for 10 min, followed by 40 cycles of 95 $^{\circ}$ C for 15 min and 60 °C for 1 min. The gene expression TaqMan® assays (Thermo Fisher Scientific, Waltham, Massachusetts, USA) used for this study were: Atxn2 (Mm01199894_m1), Atxn2l (Mm00805548_m1), Cux1 (Mm01195598 m1), Dclk1 (Mm01545304 m1), Nufip1 (Mm00479126 m1), Nufip2 (Mm01077988 m1). Syne1 (Mm04238399 m1), and Syne2 (Mm00621101 m1). The data were analyzed via the $2^{-\Delta\Delta Ct}$ method (Livak and Schmittgen, 2001), using Tbp (Mm00446973 m1) as housekeeping transcript.

2.9. Statistics and graphical presentation

Unpaired Student t-tests with Welch's correction were used to establish comparisons for continuous variables between homozygous Atxn2-CAG100-KIN and WT animals. Bar charts depicting the mean and standard deviation (S.D.) values were used for data visualization. GraphPad (Version 10.4.1, for Windows, GraphPad Prism, Boston, MA) software was used for all statistical analyses and Volcano plot generation. Significance was assumed at p<0.05 and highlighted with asterisks: *p<0.05, **p<0.01, ***p<0.001.

3. Results

3.1. Coimmunoprecipitation of ATXN2L interactors in WT versus ATXN2L-null MEFs shows novel interactions, stronger than the known LSM12, ATXN2, PABPC1 and G3BP2 associations

To identify the strongest ATXN2L interactors inside and outside RNA granules, we used previously described MEF derived from mice with constitutive deletion of *Atxn2l* exons 5-8 (Key et al., 2020). Co-IP pulling

was done with a polyclonal antibody against human ATXN2L residues 456-547 (Invitrogen, PA5-59601) or with unspecific immunoglobulin-G as negative control (IgG control, Cell Signaling Technology, #2729S). Comparisons were performed of unstressed WT MEF versus NaARS-stressed WT MEF, and of WT versus homozygous ATXN2L-null MEF. Preliminary immunoblot analysis of these samples (1000 µg each) with antibodies against human ATXN2L residues 712-Cterm (Proteintech, 24822-1-AP) demonstrated the expected presence of ATXN2L with its known interactor PABPC1 (Figure 1).

After identifying and quantifying the polypeptide components of these coimmunoprecipitates via LC-MS/MS and MaxQuant software (Table S1), 29 proteins were found associated with ATXN2L in unstressed WT, but neither in IgG ctrl nor ATXN2L-null samples (Table 1), as the most credible candidates. In comparison with the known ATXN2L cytosolic interactors and SG components ATXN2, PABPC1 and G3BP2, 24 proteins had higher abundances that approached the high concentration of ATXN2L (Table 1) and were therefore more likely candidates for equimolar binding. Prominently, the levels of label-free quantification (LFQ) as approximate reflection of protein abundance identified RNA-binding proteins (RBP) PABPN1, NUFIP2, MCRIP2, RBMS1, LARP1, PTBP1, FMR1, RPS20, FUBP3, MBNL2, ZMAT3, SFPQ, CSDE1, HNRNPK and HNRNPDL, to show association with ATXN2L at approximately equimolar ratios, with more or similar strength relative to known interactors such as LSM12, ATXN2, PABPC1, G3BP2, being completely absent from the KO co-IP. The only non-RNP with this pattern were the actin complex components SYNE2, LMOD1, ACTA2, FYB and GOLGA3, the nuclear histone HIST1H1C, the pore-forming immunity factor MPEG1, and the peroxidase PRDX1. Clearly, there is an enrichment of RBP and actin cytoskeleton factors, and this is in excellent agreement with published Drosophila melanogaster data implicating dATX2 in polysomal translation and in actin filaments (Satterfield and Pallanck, 2006; Satterfield et al., 2002). In the discussion below, the detailed comparison of ATXN2L interactor candidates with relevant literature confirmed the credibility and relevance of the mass spectrometry data. Thus, these novel observations will deepen our understanding of ATXN2L functions at the molecular level, and further validation experiments were done to define which of these proteins depend on ATXN2L regarding their stability.

MEF exposure to oxidative stress by administration of NaARS triggered strong increases of the protein chaperones HSPB8 / HSPA9 and

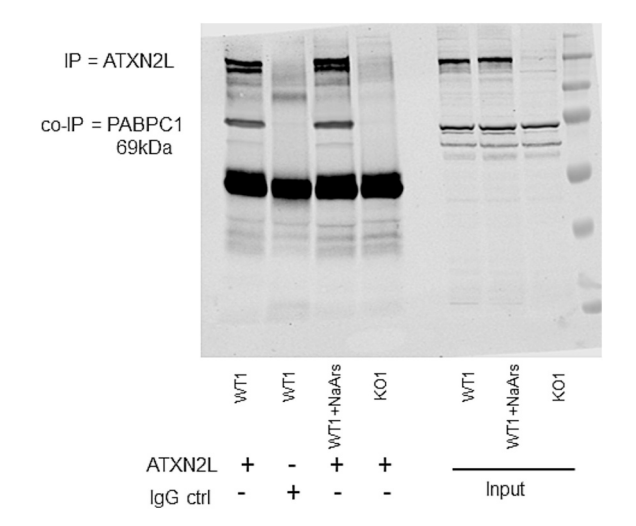


Figure 1. Immunoblot analysis of ATXN2L co-IP samples (n=1). Co-IP samples were pulled with an antibody against ATXN2L or with unspecific immunoglobulin-G as negative control (IgG). Comparisons were performed of unstressed WT MEF versus NaARS-stressed WT MEF, and of WT versus homozygous ATXN2L-null MEF. Immunoblot analysis of these samples (1000 μg each) with antibodies against ATXN2L demonstrated the expected presence of ATXN2L with its known interactor PABPC1.

the RNA chaperone HNRNPK (>2.5-fold) in the ATXN2L co-IP, in parallel to a strong decrease of SYNE2 amounts (<0.25-fold). These observations may simply reflect the reduction of RNP granules that are associated with the cytoskeletal trafficking machinery, with the concurrent induction of refolding efforts in stress granules under conditions of liquid-liquid phase separation, after cell damage.

Strong colocalization of ATXN2L and ATXN2 with NUFIP2 in stress granules induced by NaARS administration in MEF cultures was confirmed in triple immunofluorescence microscopy (Fig. S1 and S2). Thus, both biochemical and morphological observations are compatible with the notion that ATXN2L and NUFIP2 might cooperate functionally. Signal concentration around the nuclear envelope (sometimes at opposite nuclear poles where microtubule organizing centers localize and SYNE2 assembles (Zhang et al., 2009; Falk et al., 2018), see fluorescent intensity quantification in Fig. S3), lower signal intensity in nuclear substructures, and a diffuse or sometimes bundled pattern throughout the cytoplasm, with occasionally enhanced immunoreactivity at focal adhesions, was found for both ATXN2L and ATXN2 (direct comparison also in Fig. S4).

3.2. Global proteome profiling of MEF reveals NUFIP2 and SYNE2 depletion as consequence of ATXN2L absence

To document ATXN2L-null triggered downstream effects on steady state protein levels across the global proteome, we used the MEF cells again (Key et al., 2020). This unbiased survey of 5 ATXN2L-null versus 5 WT MEF lines by label free mass spectrometry achieved detection of 4386 proteins, including 280 factors that showed upregulation with nominal significance versus 292 factors with downregulation (Table S2). The most credible subset of dysregulated proteins with actual significance and at least two-fold change is shown in a volcano plot (Figure 2). As the main findings, the absence of ATXN2L causes deficiency of two of its interactors; firstly, the reduction of ATXN2L peptides to 8% caused a similar decrease to 8% for NUFIP2 (Nuclear Fragile X Mental Retardation Protein Interacting Protein 2), as DDX6-binding protein with SG localization (Ozeki et al., 2019; Jia et al., 2023). Secondly, a reduction to 12% was observed for SYNE2 peptides (also known as Nesprin-2) as actin cytoskeleton movement factor (Luxton et al., 2010; Antoku and Gundersen, 2018; Goncalves et al., 2020) that is paralogous to SYNE1 as disease gene responsible for the autosomal recessive ataxia SCAR8 (Gros-Louis et al., 2007; Synofzik et al., 2016). Otherwise, a very large and significant downregulation to 11% was found for CUX1, as a transcription factor that identifies pyramidal neurons from cortex layers II/ III (Nieto et al., 2004; Cubelos et al., 2008; Cubelos et al., 2010; Cubelos et al., 2015; Rodriguez-Tornos et al., 2016; Weiss and Nieto, 2019; Ramos et al., 2024). The biggest upregulation to 720% concerned the microtubule polymerization regulator DCLK1 that is responsible for retrograde transport and neuronal migration (Deuel et al., 2006; Shin et al., 2013; Lipka et al., 2016).

Altogether, the loss of the RBP ATXN2L in MEF destabilized NUFIP2 exclusively among its many RBP interactors, and SYNE2 prominently among the actin filament modulators. While ATXN2L did not appear essential for the other RNPs, its loss triggered a spectrum of downstream cytoskeleton dysregulations that range from actin bundling to microtubular transport, involving also vesicle dynamics.

3.3. Validation experiments by quantitative immunoblots and RT-qPCR confirm ATXN2L-null MEFs to show depleted NUFIP2/NUFIP1 protein, reduced SYNE2 protein and Cux1 mRNA, versus increased DCLK1 expression

Attempting to assess the validity of the principal findings, first the commercially available antibodies were used in quantitative immunoblots (Figure 3A) to demonstrate that two isoforms of ATXN2L near 150 kDa molecular weight were absent in mutant MEFs, while its less abundant paralog ATXN2 showed significantly elevated levels. NUFIP2

Table 1

Mass spectrometry quantifications. Mass spectrometry identification and quantification of ATXN2L co-IP components in MEF, without stress or after NaARS stress. ATXN2L and its known interactor proteins are highlighted in yellow cells; novel interactors that are absent from controls in dark grey; potential interactors with weaker ratios in light grey; protein abundance is illustrated by red background for high values and ratios above 1, while blue background illustrate ratios below 1; very low ratios are shown in dark blue.

UniProt IDs	Proteins (Gene symbols)	LFQ intensity ATXN2L- MEF-WT	ratio KO / WT	ratio IgG- ctrl / WT	ratio NaARS WT / WT	ratio KO / NaARS WT
Q3UGS4	MCRIP1	35154000	0.032	0.047	0.976	0.0331
A0A0U1RPL0;J3QP59	ATXN2L	28621000	0	0	1.212	0
Q5EBP8;P49312	HNRNPA1	26262000	0.36	0.477	1.477	0.2436
P84089;A0A1W2P7H9;A0A1W2P7T3;G3UW85	ERH	19065000	0.205	0.342	0.769	0.2671
G3UX74;G3UY42;Q8CCS6	PABPN1	12340000	0	0	1.056	0
O88569;A0A0N4SUM2	HNRNPA2B1	11152000	0	0.151	2.116	0
Q9D0R8;A0A0A0MQC9	LSM12	10838000	0.093	0.062	1.026	0.0902
E9QP46;Q6ZWQ0	SYNE2	10817000	0	0	0.168	0
O08583;G3X9I4;Q9JJW6	ALYREF;ALYREF2	8540600	0.343	0.411	0.893	0.3844
Q5F2E7	NUFIP2	7581600	0	0	0.782	0
A0A494B9L4;A0A494BBG2;A0A494B9S0;Q9CQB2	MCRIP2	5952500	0	0	1.035	0
P15864	HIST1H1C	5841200	0	0	0.744	0
E9PZ21;A0A6I8MX12	RBMS1	5189300	0	0	1.238	0
Z4YJT3;Q6ZQ58	LARP1	3731000	0	0	1.24	0
B2M1R6;P61979;H3BLL4;H3BLP7;H3BKI8;A0A286YC						
M2;A0A286YDM3;H3BK96;H3BJ43;H3BJS9;Q8BT23;A	HNRNPK					
0A286YDH1;A0A286YEC4		3718400	0	0	2.576	0
E9QM77;O70305;F6U2C2;F7B6X4;F6V8M6	ATXN2	3167000	0	0	1.783	0
E9Q279;E9QMW9;Q8CB58;P17225	PTBP1	3156900	0	0	1.168	0
E9QAT0;D3Z6U8;E9QNF5;Q6AXB7;P35922	FMR1	3084300	0	0	0.388	0
F8VPR1;Q8BVA4	LMOD1	2817100	0	0	2.163	0
P60867	RPS20	2647800	0	0	1.343	0
Q7TSC1;G3UX48	PRRC2A	2609900	0.165	0.401	1.222	0.1352
S4R294;S4R2J9;A0A0A0MQ79;Q3TLH4;S4R298;S4R2E	PRRC2C					
2;S4R2L9;S4R209	FINICZC	2367800	0	0.333	1.473	0
Q8BZN7;Q569Z6	THRAP3	2284900	0	0	1.012	0
Q60865	CAPRIN1	1970900	0	0.363	0.805	0
P62960;A2BGG7	YBX1	1859700	0	0.445	0.533	0
A0A0A6YX76;A2AJ71;A0A0A6YY39;A2AJ72;Q3TIX6	FUBP3	1717500	0	0	1.863	0
P29341;F6ZAX1	PABPC1	1695500	0	0	1.523	0
P62737;A0A494B9T3;A0A0U1RQ96	ACTA2	1642900	0	0	0.751	0
Q9JK92	HSPB8	1518000	0	0	3.038	0
E9QN37;A1L314	MPEG1	1268500	0	0	0.961	0
A0A0J9YUY8;A0A0J9YTQ8;P97379	G3BP2	1111200	0	0	1.307	0
A0A2K6EDM5;Q8C181	MBNL2	987330	0	0	2.059	0
B9EI21;O54836	ZMAT3	896930	0	0	1.02	0
Q3TGG2;E9Q5Q0	ATXN2L	892300	0	0	0.931	0
P38647	HSPA9	715080	0	0	3.408	0
Q8VIJ6	SFPQ	631580	0	0	1.623	0
A0A0G2JF72;Q8JZN2;Q91W50	CSDE1	624810	0	0	1.85	0
B1AXW5;B1AXW6;P35700;B1AXW4	PRDX1	589030	0	0	1.886	0
A0A0R4J1H6;E9QP99;P55937	GOLGA3	560160	0	0	0.995	0
НЗВКОО	HNRNPK	513110	0	0	3.058	0
D3YTQ3;F6VQH5;Q9Z130	HNRNPDL	486580	0	0	1.927	0
A0A2I3BPY6;A0A2I3BRH1;O35601	FYB	420290	0	0	1.422	0

had a depletion to 10.6%, its paralog NUFIP1 was reduced to 40.2% and SYNE2 to 61.5%, whereas DCLK1 abundance exhibited a 5-fold elevation. Antibodies against the paralog SYNE1 and against CUX1 were not sensitive or specific enough to generate convincing immunoreactivity in the MEFs.

Employing the RT-qPCR technique to test mRNA expression levels of these factors, the absence of *Atxn2l* transcript was confirmed but no upregulation of its paralog *Atxn2* was confirmed (Figure 3B), suggesting that post-transcriptional mechanisms have to be responsible for the accumulation of ATXN2 protein in ATXN2L-null MEFs. Interestingly, the depletion of NUFIP2 protein was not counteracted by its transcriptional induction, but instead accompanied by reduced *Nufip2* mRNA, suggesting that the loss-of-function of NUFIP2 is beneficial for ATXN2L-null

cells. Similarly, the reduced expression of Syne2 and Syne1 as well as Cux1 paralleled their lowered protein abundance. Conversely, a strong increase of Dclk1 transcript levels was observed to underlie the elevated DCLK1 protein abundance.

Overall, these data reproduce key findings of the proteome profile and point to a beneficial compensatory role of these dysregulations in ATXN2L-null MEFs.

3.4. The ribonucleoprotein aggregation process in the spinal cord of 14-month-old Atxn2-CAG100-KnockIn mice includes the accumulation of ATXNL2 and NUFIP2 proteins

We reasoned that the above findings may be relevant for SCA2

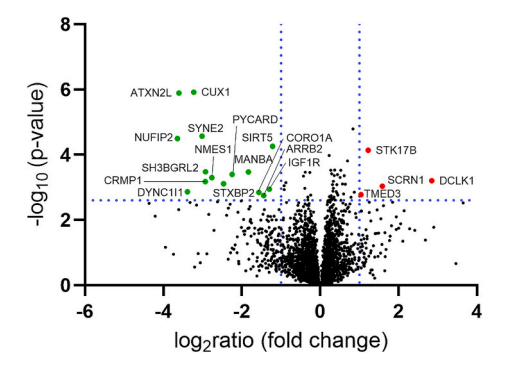


Figure 2. Volcano plot of global proteome profile of ATXN2L-null MEF cells. ATXN2L and its interactor proteins NUFIP2 / SYNE2 as well as pyramidal neuron marker CUX1 are similarly depleted, and several cytoskeletal trafficking pathway components (e.g. DYNC1I1, CRMP1, SH3BGRL2, STXBP2, and DCLK1) appear dysregulated. The position of downregulated factors on the left side was shown as green dots, upregulated factors on the right side as red dots.

disease mechanisms, in view of the known heteromultimerization of ATXN2 with ATXN2L in neuronal RNA granules during transport, and in SG. The polyO expansion within ATXN2 leads to a ribonucleoprotein aggregation process that sequestrates ribonucleoprotein interactors like PABPC1 and TDP-43 into cytosolic inclusion bodies within spinal motor neurons, possibly also within cerebellar Purkinje neurons (Elden et al., 2010; Damrath et al., 2012; Canet-Pons et al., 2021). Upon testing ATXN2L with its main protein interactors in mice with ATXN2 polyQ expansion, aged spinal cord tissues showed the previously reported reduction in translated soluble ATXN2 (Figure 4). The well-established ATXN2 aggregation process in aged spinal cord of these KIN mice (Canet-Pons et al., 2021) resulted in significant accumulation of ATXN2L (1.53-fold, p=0.0052) similar to TDP-43 (1.57-fold, p=0.003), together with NUFIP2 monomers (1.56-fold, p=0.021) and homodimers (3.28-fold, p=0.0007), SYNE1 (1.54-fold, p=0.011; SYNE2 analysis did not produce convincing immunoreactivity in these tissues, in agreement with GeneCards database proteome entries that SYNE1 but not SYNE2 is detected by mass spectrometry in spinal cord) and DCLK1 (1.25-fold, p=0.048). The sequestration of these factors into the phase-separated inclusion bodies would reduce their availability in the water-soluble cytosolic fractions. Thus, a partial loss-of-function due to aggregation or a gain-of-function due to excess amounts of these ATXN2L interactors might contribute to the cellular pathology in SCA2 via altered RNA processing and cytoskeletal dynamics.

4. Discussion

ATXN2L is essential for embryonic development in mice, indicating its crucial role in cellular survival. However, there is very limited knowledge about this protein based on patient genetics, biochemistry, microscopy studies, and bioinformatics predictions. Previously, it was thought that ATXN2L and ATXN2 function within ribonucleoprotein complexes, which are relatively stationary in the spliceosome or near the rough endoplasmic reticulum. They are believed to modulate the ribosomal translation pathway during cellular growth phases and assist in RNA quality control pathways during cellular stress and repair phases.

New evidence from this study indicates two important findings regarding ATXN2L in mice. First, the association of ATXN2L with various ribonucleoproteins is essential for NUFIP2. Second, ATXN2L interacts with SYNE2 and several other components of the actin-microtubule cytoskeleton, suggesting that it plays a role in RNA surveillance during polarized transport from the nuclear spliceosome to the tips of cell processes.

In the sections below, we will revisit our experimental data in detail and integrate it with the current literature to propose a credible scenario regarding the functions of ATXN2L.

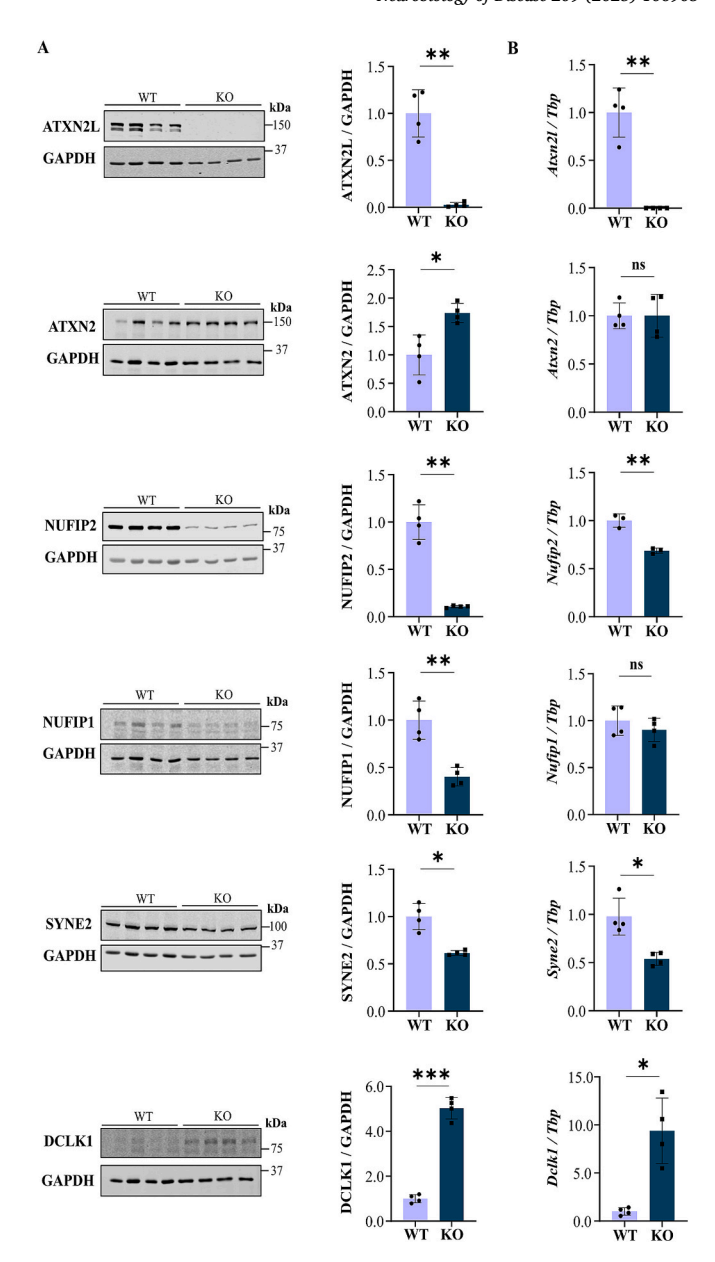


Figure 3. Validation experiments in ATXN2L-null MEFs. (A) Quantitative immunoblots document the abundances of proteins of interest in 4 mutant versus 4 WT samples, normalized to GAPDH as loading control. (B) RT-qPCR quantifies expression of transcripts of interest in 4 mutant versus 4 WT samples, normalized to Tbp mRNA as loading control. Significance was assumed at p<0.05 and highlighted with asterisks: *p<0.05, **p<0.01, ***p<0.001, ns = non-significant. Variance is shown with S.D.

4.1. Coimmunoprecipitation findings

In agreement with previous observations that ATXN2L is not exclusively cytosolic like ATXN2 (Auburger et al., 2017), but instead shows prominent nuclear localization (Kaehler et al., 2015), the ATXN2L coimmunoprecipitates contained not so much the cytosolic poly(A) binding protein PABPC1, but mainly the nuclear poly(A) binding protein PABPN1 (in control of nuclear exosomal degradation of polyadenylated RNAs) (Lemay et al., 2010; Beaulieu et al., 2012; Bresson and Conrad, 2013; Muniz et al., 2015; Meola et al., 2016), with >7-fold higher LFQ intensity as measure of abundance. Furthermore, the ATXN2L co-IP contained ZMAT3 (also known as Wig-1), which localizes mainly to the nucleolus, binding to long double-strand RNA (dsRNA) and short microRNA-like dsRNA to regulate splicing and cell senescence, while

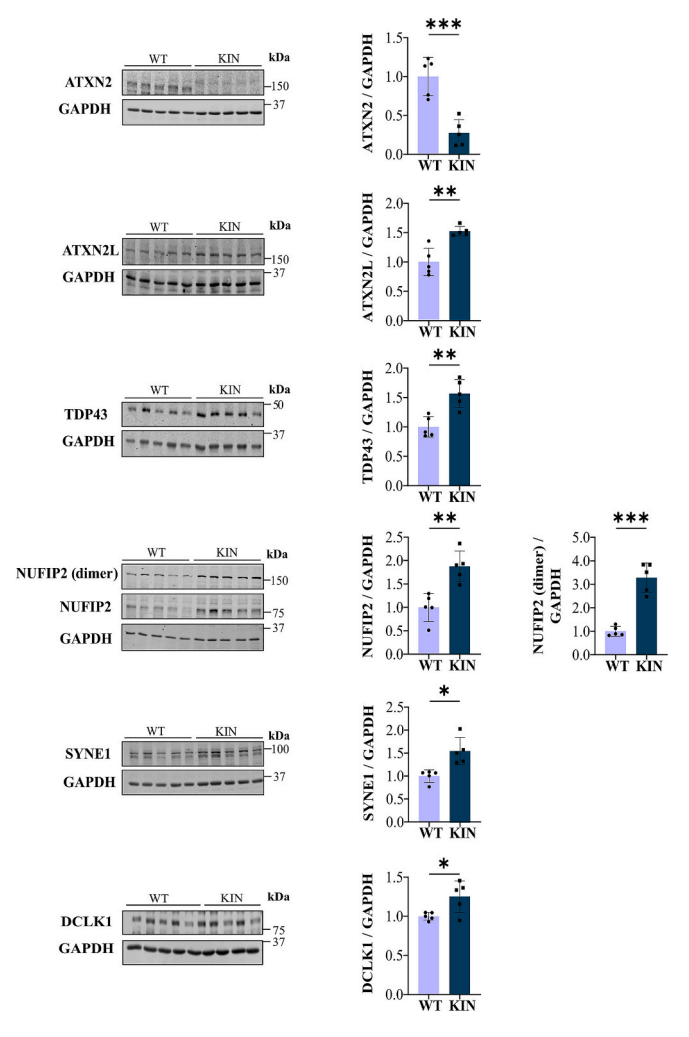


Figure 4. Validation experiments in the spinal cord of end-stage *Atxn2*-CAG100-KnockIn mice. Quantitative immunoblots demonstrating the deficiency of polyQ-expanded ATXN2 in the soluble compartment, together with accumulation of TDP-43, ATXN2L, NUFIP2 (monomers at 75 kDa, homodimers at 150 kDa), SYNE1 and DCLK1 in spinal cord homogenates from 14-month-old *Atxn2*-CAG100-KnockIn mice (graphs reflect 5 mutant versus 5 WT samples), using GAPDH as loading normalizer. Significance was assumed at p<0.05 and highlighted with asterisks: *p<0.05, **p<0.01, ***p<0.001. Variance is shown with S.D.

shuttling to the cytosol to regulate ARE-mediated RNA decay there (Vilborg et al., 2011; Kim et al., 2016; Lee et al., 2017b; Bieging-Rolett et al., 2020; Spinelli et al., 2022). In addition, the ATXN2L co-IP also comprised a subcomplex consisting of three nuclear speckle-paraspeckle proteins that modulate selective expression and translation of internal ribosomal entry site (IRES) sequences (King et al., 2014): (i) THRAP3 (also known as TRAP150), an RNA alternative splicing and nuclear RNA decay mediator, as well as R-loop resolution factor (Lee et al., 2010; Kang et al., 2021); (ii) SFPQ (also known as PSF or Polypyrimidine Tract-Binding Protein-Associated-Splicing Factor that contains a K-homology domain) as known interactor of THRAP3 and of ALS-associated NEAT1 lncRNA (Lowery et al., 2007; Hirose et al., 2014; Yarosh et al., 2015; Modic et al., 2019; Lim et al., 2020; Hogan et al., 2021); (iii) PTBP1 (also known as HNRNPI or as Polypyrimidine Tract Binding Protein 1 (Miao et al., 2022; Liu et al., 2023). Providing strong evidence for the nuclear localization of ATXN2L, the co-IP included the nuclear linker histone HIST1H1C (which is also known as H1.2, in control of cell growth versus apoptosis following DNA double-strand breaks, (Munro and La Thangue, 2017; Schnetler et al., 2020; Lai et al., 2021)). These observations implicate ATXN2L in nuclear RNA splicing and

degradation, as well as dsRNA processing, for the adaptation of cells to stress conditions.

The highest number of ATXN2L interactors were RBPs. Those with predominant localization in the nucleus included MCRIP2 (also known as FAM195A, a DDX6 interactor and SG component (Bish et al., 2015)), HNRNPK (binding to polyC sequences (Zappa et al., 2019; Yao et al., 2021)), FUBP3 (also known as MARTA2, binding 3' untranslated region UAU sequences, containing a K-homology domain (Zivraj et al., 2013; Gau et al., 2011; Mukherjee et al., 2019)), MBNL2 (as RNA alternative splicing and localization mediator, which contains a K-homology domain, binding to the ACACCC zipcode core sequence and to triplet repeat structures (Pascual et al., 2006; Taliaferro et al., 2016; Huang et al., 2023)) and HNRNPDL (also known as AU-Rich Element RNA-Binding Factor or JKTBP, (Doi et al., 1998; Kamei and Yamada, 2002; Omnus et al., 2011; Li et al., 2019)). Those with distribution throughout nucleus and cytoplasm were firstly FMR1 (Fragile X Messenger Ribonucleoprotein 1) as mRNA nuclear export / alternative splicing / dendritic transport factor that contains a K-homology domain and binds polyU sequences, again with known SG relocalization (Coyne et al., 2015; Taha et al., 2021); secondly NUFIP2 (Nuclear FMR1 Interacting Protein 2, another DDX6 interactor and SG component (Bish et al., 2015)); thirdly LARP1 (La Ribonucleoprotein 1 Translational Regulator, again in the DDX6 interactome and SG component, (Taha et al., 2021; Chatel-Chaix et al., 2013; Mattijssen et al., 2021); and fourth RPS20 (a component of the small ribosome subunit for mRNA quality control, which acts in the nucleolus to control cell proliferation (Panas et al., 2016; Krishnan et al., 2018; Huang et al., 2020)). Mutation of mouse ATXN2 was previously shown to affect ribosomal protein abundance (Fittschen et al., 2015), but the very selective ATXN2L interaction with RPS20 is noteworthy. Binding between Ataxin-2 and DDX6 is well established from human to flies (Lee et al., 2017a), so also the enrichment of DDX6 interacting proteins in the ATXN2L co-IP is expected. Predominant cytoplasmic distribution and known SG relocalization was represented only by G3BP2 (Prentzell et al., 2021; Kipper et al., 2022; Jin et al., 2022). G3BP2 and G3BP1 are distinct from other SG proteins, since they contain SH3 domains that are expected to interact with proline-rich motifs (PRM), and indeed ATXN2L and ATXN2 homologs across phylogenesis contain at least two conserved functional PRMs (Jimenez-Lopez and Guzman, 2014; Nonis et al., 2008; Drost et al., 2013).

The LSm and LSm-AD motifs of ATXN2L act as RNA chaperone that corrects conformation without consuming ATP energy, and may interact with DDX6 as RNA helicase that corrects conformation more forcefully with energy from ATP. Therefore, it seems logical that the ATXN2L interactome is enriched in other RNA chaperones such as HNRNPI, HNRNPK, HNRNPDL (Semrad, 2011), together with additional factors that contain a K-homology domain. Already in bacteria, a cooperation between the Sm domain containing factor Hfq and the K homology domain containing factor PNPase (polyribonucleotide nucleotidyltransferase) was found crucial for riboregulation (Dendooven et al., 2021).

Overall, the ATXN2L co-IP findings above are credible and indicate that the main role of ATXN2L is focused on RNA surveillance, preferentially in the perinuclear area and along the microtubule-actin cytoskeleton.

In view of the MBNL2 role for RNA relocalization along the cyto-skeleton, it was interesting to note that the RNA-binding protein RBMS1 appeared together with cytoskeletal ACTA2 (actin alpha 2) in the ATXN2L co-IPs, with the single-strand [AU]CU[AU][AU]U-sequence binding RBMS1 known to control ACTA2 transcripts, and to influence differentiation as well as radial migration of neural progenitors (Kimura et al., 1998; Habib et al., 2022; Veeraraghavan et al., 2024). The co-IP presence of LMOD1 as actin-nucleating factor (Kostyukova, 2007; Dominguez, 2016; Nauen et al., 2020) also suggests a cytoskeleton association. The putative ATXN2L interactor SYNE2 (also known as Nesprin-2) is a component of the LINC (Linker of Nucleoskeleton and

Cytoskeleton) complex that regulates cell polarity and nuclear movement by association with dynein-dynactin, kinesin and myosin motor proteins (Zhang et al., 2009; Falk et al., 2018; Luxton et al., 2010; Goncalves et al., 2020; Dawe et al., 2009; Neumann et al., 2010; Wang et al., 2015; Arsenovic et al., 2016; Hieda et al., 2021). Therefore, SYNE2 association represents additional evidence that ATXN2L localizes near the nuclear envelope along the cytoskeleton. Furthermore, FYB (also known as ADAP) as potential ATXN2L interactor has a role in actin rearrangement (Krause et al., 2000; Kliche et al., 2006; Pauker et al., 2011). In another subcellular context that agrees with the reported Golgi localization of dATX-2 in Drosophila melanogaster (Sechi et al., 2021), GOLGA3 as a candidate ATXN2L interactor is implicated in the cell reorientation by microtubules to a position where membrane and glycoprotein delivery for neurite extension is optimized. Its mutations lead to primary ciliary dyskinesia (Di Gioia et al., 2015; Tang et al., 2019; Shamseldin et al., 2020). Overall, several putative ATXN2L interactors suggest its involvement in trafficking along the cytoskeleton, presumably together with RNA granules.

The observation of molecular chaperones is frequent in any co-IP experiment, so cytosolic HSPB8 and membrane-associated HSPA9 as heat-shock proteins need not represent a specific ATXN2L function. However, CSDE1 (also known as UNR) as Golgi-/vesicle- associated cold shock protein for RNA stem-loop binding, polypyrimidine-tract-mediated IRES-dependent translation initiation, stress granule assembly and RNA decay appears to be a specific ATXN2L interactor within the RNA surveillance pathway (Jacquemin-Sablon et al., 1994; Hunt et al., 1999; Cornelis et al., 2005; Bushell et al., 2006; Kamenska et al., 2016; Youn et al., 2018).

The ATXN2L associated PRDX1 (Peroxiredoxin 1) is an antioxidant defence factor, which would modulate SG assembly/disassembly (Neumann et al., 2009; Bertoldi, 2016).

In contrast, the identification of MPEG1 (also known as Perforin-2) in the ATXN2L interactome is unrelated to previously mentioned pathways, in view of MPEG1 localization to cytoplasmic vesicles / phagosomes / lysosomes where it forms pores to mediate bacterial destruction and the cytosolic escape of bacterial fragments (Jiao et al., 2022; Yu et al., 2022; Rodriguez-Silvestre et al., 2023). Thus, the presence of MPEG1 in the ATXN2L co-IP may represent an artefact, or may be part of stress-triggered innate immune responses to toxic dsRNA or malformed RNA.

It would be interesting to compare the interactomes of ATXN2L versus ATXN2, to elucidate the complementary roles played by each paralog. Close examination of their sequences and domain structures across phylogenesis reveals that from their protist/algae/fungal ancestors until mammalian ATXN2L an approximate length of 900 amino acids contain the typical combination of RNA processing domains, together with several proline-rich motifs for actin-association (Jimenez-Lopez and Guzman, 2014). Mammalian ATXN2 is distinct by its N-terminal additional approximately 350 amino acids that evolved since fishes/amphibian/reptiles, which include the polyQ domain and three additional proline-rich motifs. Correspondingly, only for mammalian ATXN2 several interactions with actin-endosome trafficking factors were reported by two independent groups in Germany (Nonis et al., 2008; Drost et al., 2013; Ralser et al., 2005b), and functions of mammalian ATXN2 to repress endocytosis and to promote exocytosis were functionally validated lateron by two independent teams in China (Lu et al., 2019; Bian et al., 2023). The association of mammalian ATXN2 with endosome dynamics may explain why it can localize to the Golgi apparatus and perturbate its stability (Huynh et al., 2003).

ATXN2L-null MEF proteome dysregulations:

As the main finding of this paper, NUFIP2 appeared destabilized by the loss of ATXN2L in MEF, and this mass spectrometry observation was validated in independent immunoblot experiments. This massive and selective impact was unexpected, because most ribonucleoprotein interactions within SG are promiscuous, mediated by intrinsically disordered domains (IDR) of proteins and the associated RNAs in liquid-liquid

phase separation (LLPS). Such an insight about a quite exclusive interaction points to a specific function that is performed by ATXN2L together with NUFIP2 and support from their binding partner DDX6. Again, not too much has been elucidated about the physiological roles of NUFIP2, since its initial discovery as a nuclear and cytoplasmic shuttling factor with ribosomal function within the FMR1 Fragile X protein complex with RNAs (Bardoni et al., 2003; Taha et al., 2021), and its subsequent identification as a principal component in the DDX6 protein interactome (Bish et al., 2015). On the one hand, NUFIP2 was observed to bind mRNAs within their 3' untranslated region (Rehage et al., 2018), and similarly Ataxin-2 was also shown to target the 3'UTR (Yokoshi et al., 2014), in particular AU-rich elements (ARE) that are frequent in growth-regulating mRNAs (Otsuka et al., 2021). On the other hand, NUFIP2 is recruited to lysosomes (together with G3BP1 and GABARAPs of the mATG8 family) where it inactivates MTOR (Jia et al., 2023; Jia et al., 2022), and again Ataxin-2 in yeast, worms and mice was reported to repress MTOR (Bar et al., 2016; Lastres-Becker et al., 2016; DeMille et al., 2015; Yang et al., 2019; Kato et al., 2019; Prouteau and Loewith, 2019). Thus, current literature confirms that both NUFIP2 and ATXN2L are inhibitors of growth signals, and both mediate this effect by binding to specific sequences shortly upstream the poly(A) tail of mRNAs. Given that NUFIP2 sequence does not show any specific protein domain structures that would bind ATXN2L motifs, their interaction is presumably indirect in a ribonucleoprotein complex, mediated only by docking at RNAs that are recognized simultaneously by both factors. The fact that NUFIP2 is downregulated also at its transcript levels in ATXN2L-null fibroblasts suggests efforts to counteract ATXN2 loss-offunction by reducing its crucial antagonist. In view of NUFIP2 being recently identified as co-factor of Roquin in the promotion of RNA decay, acting at tandem non-canonical stem-loops within the 3'-UTR of mRNAs (Rehage et al., 2018), our findings are compatible with the notion that ATXN2L functions as RNA stabilization, survey and repair

Except for NUFIP2 depletion, the other proteome dysregulations did not include RNPs. Instead, they affected multiple cytoskeletal transport factors, among which the actin cytoskeleton movement factor SYNE2 plays the key role as ATXN2L interactor. SYNE2 was depleted in parallel to ATXN2L, and again this mass spectrometry observation was validated by immunoblot experiments. SYNE2 (aka Nesprin-2) is crucial for the tethering of nuclei and their relocation within polarized cells (Falk et al., 2018; Goncalves et al., 2020; Arsenovic et al., 2016; Hieda et al., 2021; Cartwright and Karakesisoglou, 2014; Lim et al., 2021; Woychek and Jones, 2019; Young et al., 2021; Zhou et al., 2024), so its depletion possibly underlies the increased presence of giant multinucleated cells in the ATXN2L-null MEF lines (Key et al., 2020). Given that our immunocytochemistry images showed ATXN2L concentrated at perinuclear sites where SYNE2 interacts with pericentrin at microtubule organizing centers (MTOC) (Falk et al., 2018; Goncalves et al., 2020), the question arises how this association is mediated. Thus, it is noteworthy that the SYNE2 N-terminus is structured as calponin-homology (CH) domain, and Ataxin-2 was previously shown to bind two proteins with actinbinding CH domains (Ralser et al., 2005b; Eich et al., 2019). Thus, ATXN2L may stabilize an outer nuclear envelope complex between SYNE2, the perinuclear actin cap, and the MTOC sites (Woroniuk et al., 2018; Wu et al., 2018; Crisp et al., 2006), which act with the Golgi apparatus to determine polarity of neurite outgrowth and focal adhesion (Hieda et al., 2021; Zheng et al., 2020; Schneider et al., 2011; Roux et al., 2009; Vergarajauregui et al., 2020; Kobayashi et al., 2006; Beck, 2005; Chee et al., 2023; Denis et al., 2021; Revach et al., 2015). This study observed that SYNE2 is downregulated also at transcript level upon ATXN2L loss-of-function. This finding is compatible with the notion that cells weaken SYNE2 as mechanical basis for nuclear translocation, neurite extension, and focal adhesions, when ATXN2Lmediated surveillance and repair of RNAs along microtubules is impaired. SYNE2 is key for the migration and differentiation of postmitotic cortical neurons (Yi et al., 2023; David et al., 2019), and this

indirect effect may contribute to our previous report that ATXN2L-null mice die *in utero* with a phenotype of deficient cortex lamination and neuronal apoptosis (Key et al., 2020). In this context, the down-regulation of the nuclear transcription factor CUX1, which is selectively expressed in cortical layer II/III neurons, may also contribute to the embryonic lethality of ATXN2L-null mice and perhaps to the motor neuron degeneration during postnatal life of SCA2 patients (Nieto et al., 2004; Cubelos et al., 2008; Cubelos et al., 2010; Cubelos et al., 2015; Rodriguez-Tornos et al., 2016; Weiss and Nieto, 2019; Ramos et al., 2024). Although a specific and sensitive antibody to detect CUX1 was not available to us, its decreased mRNA expression levels could be demonstrated in validation experiments.

Downstream indirect effects in the proteome, which may represent pathology effectors or act in compensatory manner, include dysregulations of the microtubule-binding growth cone collapse factor CRMP1 (Yamashita and Goshima, 2012), the actin/spectrin interactor and migration modulator SH3BGRL2 (Li et al., 2020; Li et al., 2023), the RNA granule retrograde motor DYNC111 (Liu et al., 2016; Lang et al., 2021), the actin/vesicle dynamics modulator STXBP2 (also known as MUNC18B) (Kurps and de Wit, 2012), the cytoskeleton-associated membrane protrusion factor CORO1A (Alvarez Julia et al., 2016), the cofilin scaffold ARRB2 (Zoudilova et al., 2010), the myosin light chain regulator STK17B (also known as DRAK2, implicated in several spinocerebellar ataxias (Kuwahara et al., 2003; Wu and Kapfhammer, 2022)), the cytoskeletal transport vesicle component TMED3 (Navarro and Chamberlin, 2023), the vesicle dynamics modulator SCRN1 (Lindhout et al., 2019), and the microtubule polymerization regulator DCLK1.

Importantly, downregulation of IGF1R as insulin-like growth factor 1 receptor tyrosine kinase was also documented. This observation is in line with the known Ataxin-2 modulation of MTOR growth signals, and it is noteworthy that a loss of function in IGF1R also leads to intrauterine lethality (Abuzzahab et al., 2003). The reduction of the mitochondrial deacylase SIRT5 as metabolism modulator in dependence on nutrient availability (Chalkiadaki and Guarente, 2012; Pirinen et al., 2012; Sack and Finkel, 2012) also suggests altered MTOR signals. MTOR can localize at lysosomes to sense nutrient availability and is coregulated with lysosomal enzymes, explaining the downregulation of MANBA as lysosomal mannosidase beta A, which is particularly abundant in adherent fibroblasts.

Finally, the proteome profile also exhibited downregulations of two factors implicated in inflammatory responses to bacterial infections or mitochondrial dysfunction. PYCARD contributes to innate immune response as integral adapter in inflammasome assembly which activates caspase-1 leading to secretion of pro-inflammatory cytokines (Matyszewski et al., 2018; Matyszewski et al., 2021; de Souza et al., 2021). NMES1 (aka COXFA4L3, MOCCI, or C15ORF58 in human) consists of only 83 amino acids that are localized to intracellular organelles that contain DNA and RNA in high concentration (nucleus and mitochondria). It is paralogous to mitochondrial respiratory chain factor NDUFA4 and was found to modulate cytochrome C oxidase during inflammation, so it is also known as Antiviral Mitochondrial Stress Response factor (Endou et al., 2020; Lee et al., 2021; Clayton et al., 2021; Xiong et al., 2024). Via this modulation, it also induces stressdependent lysosomal-autophagosomal degradation, upregulates glutathione as antioxidative protection factor, and enhances survival (Takakura et al., 2024).

Thus, the proteome profile of MEF cells shows that the loss of ATXN2L leads to the depletion of its protein interactors NUFIP2 and SYNE2, and to strong indirect downstream protein regulations in the cytoskeletal transport machinery, in MTOR-dependent growth pathways, and in inflammation responses, but not in the RNA processing apparatus.

It was unexpected to find ATXN2L-null mutation to cause ATXN2 accumulation, since reciprocal regulations between the two paralogs were not known so far. The apparently post-transcriptional mechanism might reflect a general unspecific effect on many factors, due to altered

RNA processing in the nucleus, or altered RNA trafficking, repair, and translation in the cytosol. It is also possible that post-translational mechanisms are underlying this effect, e.g. post-translational modifications such as phosphorylations that regulate redistribution, conformation, interactions, degradation. As a post-translational and highly specific mechanism, it is conceivable that the loss of ATXN2L is sensed and leads to a compensatorily reduced activity of a degradation enzyme that targets ATXN2L but also ATXN2. We have preliminary unpublished data that polyQ expansions in murine ATXN2 triggers specific dysregulations in the ATXN2L phosphorylation profile, so mutual influences between the two paralogs seem to exist, beyond their ability to heterodimerize.

4.2. Atxn2-CAG100-KnockIn pathogenesis involves protein accumulations

Current literature about the ATXN2 aggregation process that triggers neurodegeneration in SCA2 and ALS has paid much attention to the observation that TDP-43 is sequestrated as a factor that is essential for embryonic life (Elden et al., 2010; Becker et al., 2017; Canet-Pons et al., 2021; Sephton et al., 2010), and suggested the importance of abnormal ribonucleoprotein interactions and RNA toxicity in these diseases (Li et al., 2013; Taylor et al., 2016; McEachin et al., 2020). It was not appreciated that significant accumulation affects also the ribonucleoprotein ATXN2L as an abundant ATXN2 interactor, which is also essential for embryonic life (Key et al., 2020), together with the ribonucleoprotein NUFIP2 and probably DDX6 as well. This sequestration is likely to trigger a partial loss-of-function for these ribonucleoproteins, thus impairing neuronal maintenance and survival. Moreover, the novel findings about accumulations of SYNE1 and DCLK1 protein in the aged spinal cord of Atxn2-CAG100-KIN mice provide additional evidence that altered cytoskeletal dynamics may contribute to the disease process in SCA2 and ALS. This concept is in agreement with recent discoveries of ALS genes that function in cytoskeletal integrity and axonal transport (Dulski et al., 1993; Ghasemi and Brown Jr., 2018; Chia et al., 2018).

5. Conclusions

The present study provides evidence that the poorly characterized ribonucleoprotein ATXN2L associates with numerous other ribonucleoproteins, of which only NUFIP2 depends on its presence. Downstream indirect consequences of ATXN2L loss have been shown to affect the cytoskeletal dynamics, mTOR-dependent growth pathways, and inflammation responses. The polyQ expansion of ATXN2 leads to an excess accumulation of ribonucleoproteins ATXN2L / NUFIP2 and of cytoskeletal factors SYNE1 / DCLK1, a finding with relevance to neurodegenerative diseases like SCA2 and ALS.

Supplementary data to this article can be found online at https://doi. org/10.1016/j.nbd.2025.106903.

CRediT authorship contribution statement

Jana Key: Writing – review & editing, Writing – original draft, Visualization, Resources, Investigation, Formal analysis. Luis-Enrique Almaguer-Mederos: Writing – review & editing, Writing – original draft, Visualization, Validation, Methodology, Investigation, Formal analysis. Arvind Reddy Kandi: Writing – review & editing, Visualization, Validation, Methodology, Investigation. Nesli-Ece Sen: Writing – review & editing, Resources. Suzana Gispert: Writing – review & editing, Supervision, Resources, Methodology, Conceptualization. Gabriele Köpf: Validation, Methodology, Investigation. David Meierhofer: Writing – review & editing, Resources, Investigation, Data curation. Georg Auburger: Writing – review & editing, Writing – original draft, Visualization, Supervision, Project administration, Funding acquisition, Formal analysis, Data curation, Conceptualization.

Institutional review board statement

The study was conducted in accordance with the Declaration of Helsinki. The animal study protocol was approved by the Regier-ungspräsidium Darmstadt (V54-19c20/15-FK/1083, on 11 March 2019).

Funding

The study was funded by the Deutsche Forschungsgemeinschaft (DFG AU96/21-1).

Declaration of competing interest

The authors report no competing interests.

Acknowledgements

We thank Beata Lukaszewska-McGreal for proteome sample preparation and the Max Planck Society for support.

Data availability

All proteome data were deposited in PRIDE with accession numbers PXD061048, and PXD061161.

References

- Abdelhamid, M.A.S., Gates, A.J., Waller, Z.A.E., 2019. Destabilization of i-Motif DNA at neutral pH by G-Quadruplex ligands. Biochemistry 58 (4), 245–249.
- Abuzzahab, M.J., et al., 2003. IGF-I receptor mutations resulting in intrauterine and postnatal growth retardation. N. Engl. J. Med. 349 (23), 2211–2222.
- Akter, K.A., et al., 2017. FAM98A associates with DDX1-C14orf166-FAM98B in a novel complex involved in colorectal cancer progression. Int. J. Biochem. Cell Biol. 84, 1–13
- Albrecht, M., Lengauer, T., 2004. Survey on the PABC recognition motif PAM2. Biochem. Biophys. Res. Commun. 316 (1), 129–138.
- Al-Ramahi, I., et al., 2007. dAtaxin-2 mediates expanded Ataxin-1-induced neurodegeneration in a Drosophila model of SCA1. PLoS Genet. 3 (12), e234.
- Alvarez Julia, A., Frasch, A.C., Fuchsova, B., 2016. Neuronal filopodium formation induced by the membrane glycoprotein M6a (Gpm6a) is facilitated by coronin-1a, Rac1, and p21-activated kinase 1 (Pak1). J. Neurochem. 137 (1), 46–61.
- Alzahrani, F., Albatti, T.H., Alkuraya, F.S., 2021. A de novo ATXN2L variant in a child with developmental delay and macrocephaly. Am. J. Med. Genet. A 185 (3), 949–951.
- Amado, D.A., Davidson, B.L., 2021. Gene therapy for ALS: A review. Mol. Ther. 29 (12), 3345–3358.
- Antoku, S., Gundersen, G.G., 2018. Analysis of Nesprin-2 Interaction with Its Binding Partners and Actin. Methods Mol. Biol. 1840, 35–43.
- Arsenovic, P.T., et al., 2016. Nesprin-2G, a component of the nuclear LINC complex, is subject to myosin-dependent tension. Biophys. J. 110 (1), 34–43.
- Arsovic, A., et al., 2020. Mouse Ataxin-2 expansion downregulates CamKII and other calcium signaling factors, impairing granule-purkinje neuron synaptic strength. Int. J. Mol. Sci. 21 (18).
- Auburger, G., et al., 2017. Efficient prevention of neurodegenerative diseases by depletion of starvation response factor Ataxin-2. Trends Neurosci. 40 (8), 507–516. Ayache, J., et al., 2015. P-body assembly requires DDX6 repression complexes rather
- than decay or Ataxin2/2L complexes. Mol. Biol. Cell 26 (14), 2579–2595.

 Bar, D.Z., et al., 2016. Cell size and fat content of dietary-restricted Caenorhabditis
- Bar, D.Z., et al., 2016. Cell size and fat content of dietary-restricted Caenorhabditis elegans are regulated by ATX-2, an mTOR repressor. Proc. Natl. Acad. Sci. USA 113 (32), E4620–E4629.
- Bardoni, B., et al., 2003. 82-FIP, a novel FMRP (fragile X mental retardation protein) interacting protein, shows a cell cycle-dependent intracellular localization. Hum. Mol. Genet. 12 (14), 1689–1698.
- Baumer, D., et al., 2014. FTLD-ALS of TDP-43 type and SCA2 in a family with a full Ataxin-2 polyglutamine expansion. Acta Neuropathol. 128 (4), 597–604.
- Beaulieu, Y.B., et al., 2012. Polyadenylation-dependent control of long noncoding RNA expression by the poly(A)-binding protein nuclear 1. PLoS Genet. 8 (11), e1003078. Beck, K.A., 2005. Spectrins and the Golgi. Biochim. Biophys. Acta 1744 (3), 374–382.
- Becker, L.A., et al., 2017. Therapeutic reduction of Ataxin-2 extends lifespan and reduces pathology in TDP-43 mice. Nature 544 (7650), 367–371.
- Bertoldi, M., 2016. Human peroxiredoxins 1 and 2 and their interacting protein partners; through structure toward functions of biological complexes. Protein Pept. Lett. 23 (1), 69–77.
- Bian, W., et al., 2023. A spatially defined human Notch receptor interaction network reveals Notch intracellular storage and Ataxin-2-mediated fast recycling. Cell Rep. 42 (7), 112819.

- Bieging-Rolett, K.T., et al., 2020. Zmat3 Is a key splicing regulator in the p53 tumor suppression program. Mol. Cell 80 (3), 452–469 e9.
- Bish, R., et al., 2015. Comprehensive protein interactome analysis of a key RNA Helicase: detection of novel stress granule proteins. Biomolecules 5 (3), 1441–1466.
- Boeynaems, S., et al., 2023. Poly(A)-binding protein is an Ataxin-2 chaperone that regulates biomolecular condensates. Mol. Cell 83 (12), 2020–2034 e6.
- Borrego-Hernandez, D., et al., 2024. Intermediate repeat expansion in the ATXN2 gene as a risk factor in the ALS and FTD Spanish population. Biomedicines 12 (2).
- Bravo, J., et al., 2005. Four distinct classes of proteins as interaction partners of the PABC domain of Arabidopsis thaliana Poly(A)-binding proteins. Mol. Gen. Genomics. 272 (6), 651–665.
- Bresson, S.M., Conrad, N.K., 2013. The human nuclear poly(a)-binding protein promotes RNA hyperadenylation and decay. PLoS Genet. 9 (10), e1003893.
- Bushell, M., et al., 2006. Polypyrimidine tract binding protein regulates IRES-mediated gene expression during apoptosis. Mol. Cell 23 (3), 401–412.
- Bux, J., et al., 2023. TR-FRET-Based immunoassay to measure Ataxin-2 as a target engagement marker in spinocerebellar ataxia type 2. Mol. Neurobiol. 60 (6), 3553–3567.
- Canet-Pons, J., et al., 2021. Atxn2-CAG100-KnockIn mouse spinal cord shows progressive TDP43 pathology associated with cholesterol biosynthesis suppression. Neurobiol. Dis. 152, 105289.
- Cartwright, S., Karakesisoglou, I., 2014. Nesprins in health and disease. Semin. Cell Dev. Biol. 29, 169–179.
- Casse, F., et al., 2023. Detection of ATXN2 expansions in an exome dataset: an underdiagnosed cause of parkinsonism. Mov. Disord Clin. Pract. 10 (4), 664–669.
- Chalkiadaki, A., Guarente, L., 2012. Sirtuins mediate mammalian metabolic responses to nutrient availability. Nat. Rev. Endocrinol. 8 (5), 287–296.
- Charles, P., et al., 2007. Are interrupted SCA2 CAG repeat expansions responsible for parkinsonism? Neurology 69 (21), 1970–1975.
- Chatel-Chaix, L., et al., 2013. A host YB-1 ribonucleoprotein complex is hijacked by hepatitis C virus for the control of NS3-dependent particle production. J. Virol. 87 (21), 11704–11720.
- Li Mow Chee, F., et al., 2023. Mena regulates nesprin-2 to control actin-nuclear lamina associations, trans-nuclear membrane signalling and gene expression. Nat. Commun. 14 (1), 1602.
- Chen, C.Y., Shyu, A.B., 1995. AU-rich elements: characterization and importance in mRNA degradation. Trends Biochem. Sci. 20 (11), 465–470.
- Chia, R., Chio, A., Traynor, B.J., 2018. Novel genes associated with amyotrophic lateral sclerosis: diagnostic and clinical implications. Lancet Neurol. 17 (1), 94–102.
- Ciosk, R., DePalma, M., Priess, J.R., 2004. ATX-2, the C. elegans ortholog of ataxin 2, functions in translational regulation in the germline. Development 131 (19), 4831–4841.
- Clayton, S.A., et al., 2021. Inflammation causes remodeling of mitochondrial cytochrome c oxidase mediated by the bifunctional gene C15orf48. Sci. Adv. 7 (50) eabl5182.
- Corbet, G.A., Parker, R., 2019. RNP Granule Formation: Lessons from P-Bodies and Stress Granules. Cold Spring Harb. Symp. Quant. Biol. 84, 203–215.
- Cornelis, S., et al., 2005. UNR translation can be driven by an IRES element that is negatively regulated by polypyrimidine tract binding protein. Nucleic Acids Res. 33 (10), 3095–3108.
- Coyne, A.N., et al., 2015. Fragile X protein mitigates TDP-43 toxicity by remodeling RNA granules and restoring translation. Hum. Mol. Genet. 24 (24), 6886–6898.
- Crisp, M., et al., 2006. Coupling of the nucleus and cytoplasm: role of the LINC complex. J. Cell Biol. 172 (1), 41–53.
- Cubelos, B., et al., 2008. Cux-1 and Cux-2 control the development of Reelin expressing cortical interneurons. Dev. Neurobiol. 68 (7), 917–925.
- Cubelos, B., et al., 2010. Cux1 and Cux2 regulate dendritic branching, spine morphology, and synapses of the upper layer neurons of the cortex. Neuron 66 (4), 523–535.
- and synapses of the upper layer neurons of the cortex. Neuron 66 (4), 523–535. Cubelos, B., et al., 2015. Cux1 and Cux2 selectively target basal and apical dendritic compartments of layer II-III cortical neurons. Dev. Neurobiol. 75 (2), 163–172.
- Damrath, E., et al., 2012. ATXN2-CAG42 sequesters PABPC1 into insolubility and induces FBXW8 in cerebellum of old ataxic knock-in mice. PLoS Genet. 8 (8), e1002920.
- David, B.G., et al., 2019. Linking substrate and nucleus via actin cytoskeleton in pluripotency maintenance of mouse embryonic stem cells. Stem Cell Res. 41, 101614.
- Dawe, H.R., et al., 2009. Nesprin-2 interacts with meckelin and mediates ciliogenesis via remodelling of the actin cytoskeleton. J. Cell Sci. 122 (Pt 15), 2716–2726.
- de Souza, J.G., Starobinas, N., Ibanez, O.C.M., 2021. Unknown/enigmatic functions of extracellular ASC. Immunology 163 (4), 377–388.
- Del Castillo, U., et al., 2019. Conserved role for Ataxin-2 in mediating endoplasmic reticulum dynamics. Traffic 20 (6), 436–447.
- Del Castillo, U., et al., 2022. Ataxin-2 is essential for cytoskeletal dynamics and neurodevelopment in Drosophila. iScience 25 (1), 103536.
- DeMille, D., et al., 2015. PAS kinase is activated by direct SNF1-dependent phosphorylation and mediates inhibition of TORC1 through the phosphorylation and activation of Pbp1. Mol. Biol. Cell 26 (3), 569–582.
- Dendooven, T., et al., 2021. A cooperative PNPase-Hfq-RNA carrier complex facilitates bacterial riboregulation. Mol. Cell 81 (14), 2901–2913 e5.
- Denis, K.B., et al., 2021. The LINC complex is required for endothelial cell adhesion and adaptation to shear stress and cyclic stretch. Mol. Biol. Cell 32 (18), 1654–1663.
- Deuel, T.A., et al., 2006. Genetic interactions between doublecortin and doublecortinlike kinase in neuronal migration and axon outgrowth. Neuron 49 (1), 41–53.
- Dhaliwal, J.S., et al., 2022. An RNA granule for translation quality control in Saccharomyces cerevisiae. J. Cell Sci. 135 (23).

- Di Gioia, S.A., et al., 2015. Interactome analysis reveals that FAM161A, deficient in recessive retinitis pigmentosa, is a component of the Golgi-centrosomal network. Hum. Mol. Genet. 24 (12), 3359–3371.
- Doi, A., et al., 1998. Molecular cloning of the cDNA encoding A + U-rich element RNA binding factor. Biochim. Biophys. Acta 1396 (1), 51–56.
- Dominguez, R., 2016. The WH2 domain and actin nucleation: necessary but insufficient. Trends Biochem. Sci. 41 (6), 478–490.
- Drost, J., et al., 2013. Ataxin-2 modulates the levels of Grb2 and SRC but not ras signaling. J. Mol. Neurosci. 51 (1), 68–81.
- Dulski, J., Konno, T., Wszolek, Z., 1993. In: Adam, M.P., et al. (Eds.), DCTN1-Related Neurodegeneration, in GeneReviews((R)). Seattle (WA).
- Eich, F., et al., 2019. Ataxin-2 Binds Alpha-Actinin-1. Preprints.org, 201911.0399.
 Elaswad, M.T., et al., 2022. Large RNP granules in Caenorhabditis elegans oocytes have distinct phases of RNA-binding proteins. G3 (Bethesda) 12 (9).
- Elden, A.C., et al., 2010. Ataxin-2 intermediate-length polyglutamine expansions are associated with increased risk for ALS. Nature 466 (7310), 1069–1075.
- Endou, M., et al., 2020. Coxfa4l3, a novel mitochondrial electron transport chain Complex 4 subunit protein, switches from Coxfa4 during spermatogenesis. Mitochondrion 52, 1–7.
- Estrada, R., et al., 1999. Spinocerebellar ataxia 2 (SCA2): morphometric analyses in 11 autopsies. Acta Neuropathol. 97 (3), 306–310.
- Falk, N., et al., 2018. Functional analyses of Pericentrin and Syne-2 interaction in ciliogenesis. J. Cell Sci. 131 (16).
- Felicio, D., et al., 2023. Functional implications of paralog genes in polyglutamine spinocerebellar ataxias. Hum. Genet. 142 (12), 1651–1676.
- Fittschen, M., et al., 2015. Genetic ablation of Ataxin-2 increases several global translation factors in their transcript abundance but decreases translation rate. Neurogenetics 16 (3), 181–192.
- Freibaum, B.D., et al., 2021. High-fidelity reconstitution of stress granules and nucleoli in mammalian cellular lysate. J. Cell Biol. 220 (3).
- Gau, B.H., et al., 2011. FUBP3 interacts with FGF9 3' microsatellite and positively regulates FGF9 translation. Nucleic Acids Res. 39 (9), 3582–3593.
- Ghasemi, M., Brown Jr., R.H., 2018. Genetics of amyotrophic lateral sclerosis. Cold Spring Harb. Perspect. Med. 8 (5).
- Gielisch, I., Meierhofer, D., 2015. Metabolome and proteome profiling of complex I deficiency induced by rotenone. J. Proteome Res. 14 (1), 224–235.
- Gispert, S., et al., 2012. The modulation of Amyotrophic Lateral Sclerosis risk by Ataxin-2 intermediate polyglutamine expansions is a specific effect. Neurobiol. Dis. 45 (1), 356–361.
- Glass, J.D., et al., 2022. ATXN2 intermediate expansions in amyotrophic lateral sclerosis. Brain 145 (8), 2671–2676.
- Gnazzo, M.M., et al., 2016. The RNA-binding protein ATX-2 regulates cytokinesis through PAR-5 and ZEN-4. Mol. Biol. Cell 27 (20), 3052–3064.
- Goncalves, J.C., et al., 2020. Nesprin-2 recruitment of BicD2 to the nuclear envelope controls dynein/kinesin-mediated neuronal migration in vivo. Curr. Biol. 30 (16), 3116–3129 e4.
- Gros-Louis, F., et al., 2007. Mutations in SYNE1 lead to a newly discovered form of autosomal recessive cerebellar ataxia. Nat. Genet. 39 (1), 80–85.
- Guerrero, E.N., et al., 2016. TDP-43/FUS in motor neuron disease: complexity and challenges. Prog. Neurobiol. 145-146, 78–97.
- Habib, K., et al., 2022. RNA binding protein Rbms1 enables neuronal differentiation and radial migration during neocortical development by binding and stabilizing the RNA message for Efr3a. Mol. Cell 45 (8), 588–602.
- Halbach, M.V., et al., 2015. Both ubiquitin ligases FBXW8 and PARK2 are sequestrated into insolubility by ATXN2 PolyQ expansions, but only FBXW8 expression is dysregulated. PLoS One 10 (3), e0121089.
- Halbach, M.V., et al., 2017. Atxn2 Knockout and CAG42-Knock-in cerebellum shows similarly dysregulated expression in calcium homeostasis pathway. Cerebellum 16 (1), 68–81.
- Hardwick, S.W., Luisi, B.F., 2013. Rarely at rest: RNA helicases and their busy contributions to RNA degradation, regulation and quality control. RNA Biol. 10 (1), 56–70.
- Hieda, M., et al., 2021. The SUN2-nesprin-2 LINC complex and KIF20A function in the Golgi dispersal. Sci. Rep. 11 (1), 5358.
- Hirose, T., et al., 2014. NEAT1 long noncoding RNA regulates transcription via protein sequestration within subnuclear bodies. Mol. Biol. Cell 25 (1), 169–183.
- Hogan, A.L., et al., 2021. Splicing factor proline and glutamine rich intron retention, reduced expression and aggregate formation are pathological features of amyotrophic lateral sclerosis. Neuropathol. Appl. Neurobiol. 47 (7), 990–1003.
- Huang, H., Ghalei, H., Karbstein, K., 2020. Quality control of 40S ribosome head assembly ensures scanning competence. J. Cell Biol. 219 (11).
- Huang, C.W., et al., 2023. Muscleblind-like 2 knockout shifts adducin 1 isoform expression and alters dendritic spine dynamics of cortical neurons during brain development. Neuropathol. Appl. Neurobiol. 49 (2), e12890.
- Hunt, S.L., et al., 1999. unr, a cellular cytoplasmic RNA-binding protein with five cold-shock domains, is required for internal initiation of translation of human rhinovirus RNA. Genes Dev. 13 (4), 437–448.
- Huynh, D.P., et al., 2003. Expansion of the polyQ repeat in Ataxin-2 alters its Golgi localization, disrupts the Golgi complex and causes cell death. Hum. Mol. Genet. 12 (13), 1485–1496.
- Imbert, G., et al., 1996. Cloning of the gene for spinocerebellar ataxia 2 reveals a locus with high sensitivity to expanded CAG/glutamine repeats. Nat. Genet. 14 (3), 285–291.
- Inagaki, H., et al., 2020. Direct evidence that Ataxin-2 is a translational activator mediating cytoplasmic polyadenylation. J. Biol. Chem. 295 (47), 15810–15825.

- Inagaki, H., Hosoda, N., Hoshino, S.I., 2021. DDX6 is a positive regulator of Ataxin-2/ PAPD4 cytoplasmic polyadenylation machinery. Biochem. Biophys. Res. Commun. 553, 9-16.
- Jacquemin-Sablon, H., et al., 1994. Nucleic acid binding and intracellular localization of unr, a protein with five cold shock domains. Nucleic Acids Res. 22 (13), 2643–2650.
- Jia, J., et al., 2022. Stress granules and mTOR are regulated by membrane atg8ylation during lysosomal damage. J. Cell Biol. 221 (11).
- Jia, J., et al., 2023. Membrane Atg8ylation, stress granule formation, and MTOR regulation during lysosomal damage. Autophagy 19 (6), 1893–1895.
- Jiao, F., et al., 2022. Perforin-2 clockwise hand-over-hand pre-pore to pore transition mechanism. Nat. Commun. 13 (1), 5039.
- Jimenez-Lopez, D., Guzman, P., 2014. Insights into the evolution and domain structure of Ataxin-2 proteins across eukaryotes. BMC Res. Notes 7, 453.
- Jin, G., et al., 2022. G3BP2: structure and function. Pharmacol. Res. 186, 106548.
- Kaehler, C., et al., 2012. Ataxin-2-like is a regulator of stress granules and processing bodies. PLoS One 7 (11), e50134.
- Kaehler, C., et al., 2015. PRMT1-mediated arginine methylation controls ATXN2L localization. Exp. Cell Res. 334 (1), 114–125.
- Kamei, D., Yamada, M., 2002. Interactions of heterogeneous nuclear ribonucleoprotein D-like protein JKTBP and its domains with high-affinity binding sites. Gene 298 (1), 49–57.
- Kamenska, A., et al., 2016. The DDX6-4E-T interaction mediates translational repression and P-body assembly. Nucleic Acids Res. 44 (13), 6318–6334.
- Kang, H.J., et al., 2021. Thrap3 promotes R-loop resolution via interaction with methylated DDX5. Exp. Mol. Med. 53 (10), 1602–1611.
- Kaplanis, J., et al., 2020. Evidence for 28 genetic disorders discovered by combining healthcare and research data. Nature 586 (7831), 757–762.
- Kato, M., et al., 2019. Redox state controls phase separation of the yeast Ataxin-2 protein via reversible oxidation of its methionine-rich low-complexity domain. Cell 177 (3), 711–721 e8.
- Key, J., et al., 2020. Mid-Gestation lethality of Atxn2l-Ablated Mice. Int. J. Mol. Sci. 21 (14).
- Kiehl, T.R., Shibata, H., Pulst, S.M., 2000. The ortholog of human Ataxin-2 is essential for early embryonic patterning in C. elegans. J. Mol. Neurosci. 15 (3), 231–241.
- Kiehl, T.R., et al., 2006. Generation and characterization of Sca2 (Ataxin-2) knockout mice. Biochem. Biophys. Res. Commun. 339 (1), 17–24.
- Kim, S.H., et al., 2016. Allele-specific regulation of mutant Huntingtin by Wig1, a downstream target of p53. Hum. Mol. Genet. 25 (12), 2514–2524.
- Kim, Y.E., et al., 2017. SCA2 family presenting as typical Parkinson's disease: 34 year follow up. Parkinsonism Relat. Disord. 40, 69–72.
- Kimura, K., et al., 1998. c-Myc gene single-strand binding protein-1, MSSP-1, suppresses transcription of alpha-smooth muscle actin gene in chicken visceral smooth muscle cells. Nucleic Acids Res. 26 (10), 2420–2425.
- Kimura, Y., Irie, K., Irie, K., 2013. Pbp1 is involved in Ccr4- and Khd1-mediated regulation of cell growth through association with ribosomal proteins Rpl12a and Rpl12b. Eukaryot. Cell 12 (6), 864–874.
- King, H.A., et al., 2014. Remodelling of a polypyrimidine tract-binding protein complex during apoptosis activates cellular IRESs. Cell Death Differ. 21 (1), 161–171.
- Kipper, K., Mansour, A., Pulk, A., 2022. Neuronal RNA granules are ribosome complexes stalled at the pre-translocation state. J. Mol. Biol. 434 (20), 167801.
- Kliche, S., et al., 2006. The ADAP/SKAP55 signaling module regulates T-cell receptormediated integrin activation through plasma membrane targeting of Rap1. Mol. Cell. Biol. 26 (19), 7130–7144.
- Klockgether, T., Mariotti, C., Paulson, H.L., 2019. Spinocerebellar ataxia. Nat. Rev. Dis. Primers 5 (1), 24.
- Kobayashi, Y., et al., 2006. Identification and characterization of GSRP-56, a novel Golgilocalized spectrin repeat-containing protein. Exp. Cell Res. 312 (16), 3152–3164.
- Kostyukova, A.S., 2007. Leiomodin/tropomyosin interactions are isoform specific. Arch. Biochem. Biophys. 465 (1), 227–230.
- Kozlov, G., et al., 2010. Structural basis of binding of P-body-associated proteins GW182 and Ataxin-2 by the Mlle domain of poly(A)-binding protein. J. Biol. Chem. 285 (18), 13599–13606.
- Krainer, G., et al., 2021. Reentrant liquid condensate phase of proteins is stabilized by hydrophobic and non-ionic interactions. Nat. Commun. 12 (1), 1085.
- Krause, M., et al., 2000. Fyn-binding protein (Fyb)/SLP-76-associated protein (SLAP), Ena/vasodilator-stimulated phosphoprotein (VASP) proteins and the Arp2/3 complex link T cell receptor (TCR) signaling to the actin cytoskeleton. J. Cell Biol. 149 (1), 181–194.
- Krishnan, R., Boddapati, N., Mahalingam, S., 2018. Interplay between human nucleolar GNL1 and RPS20 is critical to modulate cell proliferation. Sci. Rep. 8 (1), 11421.
- Kurps, J., de Wit, H., 2012. The role of Munc18-1 and its orthologs in modulation of cortical F-actin in chromaffin cells. J. Mol. Neurosci. 48 (2), 339–346.
- Kuwahara, H., et al., 2003. The apoptosis-inducing protein kinase DRAK2 is inhibited in a calcium-dependent manner by the calcium-binding protein CHP. J. Biochem. 134 (2), 245–250.
- Kwiatkowski Jr., T.J., et al., 2009. Mutations in the FUS/TLS gene on chromosome 16 cause familial amyotrophic lateral sclerosis. Science 323 (5918), 1205–1208.
- Kwon, Y.J., et al., 2013. Structure and expression analyses of SVA elements in relation to functional genes. Genomics Inform 11 (3), 142–148.
- Lai, S., et al., 2021. Molecular and cellular functions of the linker histone H1.2. Front. Cell Dev. Biol. 9, 773195.
- Lang, B., et al., 2021. Matrix-screening reveals a vast potential for direct protein-protein interactions among RNA binding proteins. Nucleic Acids Res. 49 (12), 6702–6721.
- Lastres-Becker, I., et al., 2008a. Insulin receptor and lipid metabolism pathology in Ataxin-2 knock-out mice. Hum. Mol. Genet. 17 (10), 1465–1481.

- Lastres-Becker, I., Rub, U., Auburger, G., 2008b. Spinocerebellar ataxia 2 (SCA2). Cerebellum 7 (2), 115–124.
- Lastres-Becker, I., et al., 2016. Mammalian Ataxin-2 modulates translation control at the pre-initiation complex via PI3K/mTOR and is induced by starvation. Biochim. Biophys. Acta 1862 (9), 1558–1569.
- Lee, K.M., Hsu Ia, W., Tarn, W.Y., 2010. TRAP150 activates pre-mRNA splicing and promotes nuclear mRNA degradation. Nucleic Acids Res. 38 (10), 3340–3350.
- Lee, T., et al., 2011. Ataxin-2 intermediate-length polyglutamine expansions in European ALS patients. Hum. Mol. Genet. 20 (9), 1697–1700.
- Lee, J., et al., 2017a. LSM12 and ME31B/DDX6 define distinct modes of posttranscriptional regulation by ATAXIN-2 protein complex in drosophila circadian pacemaker neurons. Mol. Cell 66 (1), 129–140 e7.
- Lee, H.C., et al., 2017b. WIG1 is crucial for AGO2-mediated ACOT7 mRNA silencing via miRNA-dependent and -independent mechanisms. Nucleic Acids Res. 45 (11), 6894–6910.
- Lee, C.Q.E., et al., 2021. Coding and non-coding roles of MOCCI (C15ORF48) coordinate to regulate host inflammation and immunity. Nat. Commun. 12 (1), 2130.
- Lefebvre, S., et al., 1995. Identification and characterization of a spinal muscular atrophy-determining gene. Cell 80 (1), 155–165.
- Lemay, J.F., et al., 2010. The nuclear poly(A)-binding protein interacts with the exosome to promote synthesis of noncoding small nucleolar RNAs. Mol. Cell 37 (1), 34–45.
- Li, Y.R., et al., 2013. Stress granules as crucibles of ALS pathogenesis. J. Cell Biol. 201 (3), 361–372.
- Li, P.P., et al., 2016. ATXN2-AS, a gene antisense to ATXN2, is associated with spinocerebellar ataxia type 2 and amyotrophic lateral sclerosis. Ann. Neurol. 80 (4), 600–615
- Li, R.Z., et al., 2019. hnRNPDL extensively regulates transcription and alternative splicing. Gene 687, 125–134.
- Li, D.D., et al., 2020. SH3BGRL2 exerts a dual function in breast cancer growth and metastasis and is regulated by TGF-beta1. Am. J. Cancer Res. 10 (4), 1238–1254.
- Li, P.P., et al., 2021. RNA Toxicity and Perturbation of rRNA Processing in Spinocerebellar Ataxia Type 2. Mov. Disord. 36 (11), 2519–2529.
- Li, N., et al., 2023. Structural basis of membrane skeleton organization in red blood cells.
- Cell 186 (9), 1912–1929 e18. Lim, Y.W., et al., 2020. The emerging role of the RNA-binding protein SFPQ in neuronal
- function and neurodegeneration. Int. J. Mol. Sci. 21 (19). Lim, S.M., et al., 2021. Structures of FHOD1-Nesprin1/2 complexes reveal alternate
- binding modes for the FH3 domain of formins. Structure 29 (6), 540-552 e5. Lin, L., et al., 2019. ATXN2L upregulated by epidermal growth factor promotes gastric
- cancer cell invasiveness and oxaliplatin resistance. Cell Death Dis. 10 (3), 173. Linder, B., Fischer, U., Gehring, N.H., 2015. mRNA metabolism and neuronal disease. FEBS Lett. 589 (14), 1598–1606.
- Lindhout, F.W., et al., 2019. VAP-SCRN1 interaction regulates dynamic endoplasmic reticulum remodeling and presynaptic function. EMBO J. 38 (20), e101345.
- Lipka, J., et al., 2016. Microtubule-binding protein doublecortin-like kinase 1 (DCLK1) guides kinesin-3-mediated cargo transport to dendrites. EMBO J. 35 (3), 302–318.
- Liu, Z.D., et al., 2016. Cellular model of neuronal atrophy induced by DYNC111 deficiency reveals protective roles of RAS-RAF-MEK signaling. Protein Cell 7 (9), 638–650.
- Liu, H.L., et al., 2023. The role of RNA splicing factor PTBP1 in neuronal development. Biochim. Biophys. Acta, Mol. Cell Res. 1870 (7), 119506.
- Livak, K.J., Schmittgen, T.D., 2001. Analysis of relative gene expression data using realtime quantitative PCR and the 2(-Delta Delta C(T)) Method. Methods 25 (4), 402–408.
- Lopez-Juarez, Z.M., Aguilar-Henonin, L., Guzman, P., 2021. The ATXN2 Orthologs CID3 and CID4, Act Redundantly to In-Fluence Developmental Pathways throughout the Life Cycle of Arabidopsis thaliana. Int. J. Mol. Sci. 22 (6).

 Lowery, L.A., Rubin, J., Sive, H., 2007. Whitesnake/sfpq is required for cell survival and
- Lowery, L.A., Rubin, J., Sive, H., 2007. Whitesnake/stpq is required for cell survival and neuronal development in the zebrafish. Dev. Dyn. 236 (5), 1347–1357.
- Lu, C.S., et al., 2002. Dopa-responsive parkinsonism phenotype of spinocerebellar ataxia type 2. Mov. Disord. 17 (5), 1046–1051.
- Lu, Y., et al., 2019. Internalization characterization of Si nanorod with camouflaged cell membrane proteins reveals ATXN2 as a negative regulator. Cells 8 (8).
- Luxton, G.W., et al., 2010. Linear arrays of nuclear envelope proteins harness retrograde actin flow for nuclear movement. Science 329 (5994), 956–959.
- Maine, E.M., et al., 2004. Caenorhabditis elegans atx-2 promotes germline proliferation and the oocyte fate. Genetics 168 (2), 817–830.
- Mandrioli, J., et al., 2020. ALS and FTD: Where RNA metabolism meets protein quality control. Semin. Cell Dev. Biol. 99, 183–192.
- Mangus, D.A., Amrani, N., Jacobson, A., 1998. Pbp1p, a factor interacting with Saccharomyces cerevisiae poly(A)-binding protein, regulates polyadenylation. Mol. Cell. Biol. 18 (12), 7383–7396.
- Mangus, D.A., et al., 2004. Identification of factors regulating poly(A) tail synthesis and maturation. Mol. Cell. Biol. 24 (10), 4196–4206.
- Markmiller, S., et al., 2018. Context-dependent and disease-specific diversity in protein interactions within stress granules. Cell 172 (3), 590–604 e13.
- Marmor-Kollet, H., et al., 2020. Spatiotemporal proteomic analysis of stress granule disassembly using APEX reveals regulation by SUMOylation and links to ALS pathogenesis. Mol. Cell 80 (5), 876–891 e6.
- Martens, L., et al., 2005. PRIDE: the proteomics identifications database. Proteomics 5 (13), 3537–3545.
- Mattijssen, S., et al., 2021. LARP1 and LARP4: up close with PABP for mRNA 3' poly(A) protection and stabilization. RNA Biol. 18 (2), 259–274.
- Matyszewski, M., Morrone, S.R., Sohn, J., 2018. Digital signaling network drives the assembly of the AIM2-ASC inflammasome. Proc. Natl. Acad. Sci. USA 115 (9), E1963–E1972.

- Matyszewski, M., et al., 2021. Distinct axial and lateral interactions within homologous filaments dictate the signaling specificity and order of the AIM2-ASC inflammasome. Nat. Commun. 12 (1), 2735.
- McCann, C., et al., 2011. The Ataxin-2 protein is required for microRNA function and synapse-specific long-term olfactory habituation. Proc. Natl. Acad. Sci. USA 108 (36), E655–E662.
- McEachin, Z.T., et al., 2020. RNA-mediated toxicity in C9orf72 ALS and FTD. Neurobiol. Dis. 145, 105055.
- Meierhofer, D., et al., 2016. Ataxin-2 (Atxn2)-knock-out mice show branched chain amino acids and fatty acids pathway alterations. Mol. Cell. Proteomics 15 (5), 1728–1739.
- Meola, N., et al., 2016. Identification of a nuclear exosome decay pathway for processed transcripts. Mol. Cell 64 (3), 520–533.
- Miao, H., et al., 2022. MALAT1 modulates alternative splicing by cooperating with the splicing factors PTBP1 and PSF. Sci. Adv. 8 (51) eabq7289.
- Miyaue, N., et al., 2017. DAT SPECT may have diagnostic value in prodromal SCA2 patients with parkinsonism. Parkinsonism Relat. Disord. 44, 137–141.
- Modic, M., et al., 2019. Cross-regulation between TDP-43 and paraspeckles promotes pluripotency-differentiation transition. Mol. Cell 74 (5), 951–965 e13.
- Moon, S.L., et al., 2020. Coupling of translation quality control and mRNA targeting to stress granules. J. Cell Biol. 219 (8).
- Mordovkina, D., et al., 2020. Y-Box binding proteins in mRNP assembly, Translation, and Stability Control. Biomolecules 10 (4).
- Mukherjee, J., et al., 2019. beta-Actin mRNA interactome mapping by proximity biotinylation. Proc. Natl. Acad. Sci. USA 116 (26), 12863–12872.
- Muniz, L., Davidson, L., West, S., 2015. Poly(A) Polymerase and the nuclear Poly(A) binding protein, PABPN1, coordinate the splicing and degradation of a subset of human Pre-mRNAs. Mol. Cell. Biol. 35 (13), 2218–2230.
- Munro, S., La Thangue, N.B., 2017. Linking H1 with chromatin and growth control. Mol. Cell. Oncol. 4 (6), e1360977.
- Nauen, D.W., et al., 2020. Putative autoantigen Leiomodin-1 is expressed in the human brain and in the membrane fraction of newly formed neurons. Pathogens 9 (12).
- Navarro, K.G., Chamberlin, H.M., 2023. Genetic characterization of C. elegans TMED genes. Dev. Dyn. 252 (9), 1149–1161.
- Neumann, M., et al., 2006. Ubiquitinated TDP-43 in frontotemporal lobar degeneration and amyotrophic lateral sclerosis. Science 314 (5796), 130–133.
- Neumann, C.A., Cao, J., Manevich, Y., 2009. Peroxiredoxin 1 and its role in cell signaling. Cell Cycle 8 (24), 4072–4078.
- Neumann, S., et al., 2010. Nesprin-2 interacts with alpha-catenin and regulates Wnt signaling at the nuclear envelope. J. Biol. Chem. 285 (45), 34932–34938.
- Nieto, M., et al., 2004. Expression of Cux-1 and Cux-2 in the subventricular zone and upper layers II-IV of the cerebral cortex. J. Comp. Neurol. 479 (2), 168–180.
- Nkiliza, A., et al., 2016. RNA-binding disturbances as a continuum from spinocerebellar ataxia type 2 to Parkinson disease. Neurobiol. Dis. 96, 312–322.
- Nonhoff, U., et al., 2007. Ataxin-2 interacts with the DEAD/H-box RNA helicase DDX6 and interferes with P-bodies and stress granules. Mol. Biol. Cell 18 (4), 1385–1396.
- Nonis, D., et al., 2008. Ataxin-2 associates with the endocytosis complex and affects EGF receptor trafficking. Cell. Signal. 20 (10), 1725–1739.
- Omnus, D.J., et al., 2011. JKTBP1 is involved in stabilization and IRES-dependent translation of NRF mRNAs by binding to 5' and 3' untranslated regions. J. Mol. Biol. 407 (4), 492–504.
- Otsuka, H., et al., 2021. Corrigendum: emerging evidence of translational control by AU-Rich element-binding proteins. Front. Genet. 12, 715196.
- Ozeki, K., et al., 2019. FAM98A is localized to stress granules and associates with multiple stress granule-localized proteins. Mol. Cell. Biochem. 451 (1-2), 107–115.
- Panas, M.D., Ivanov, P., Anderson, P., 2016. Mechanistic insights into mammalian stress granule dynamics. J. Cell Biol. 215 (3), 313–323.
- Pascual, M., et al., 2006. The Muscleblind family of proteins: an emerging class of regulators of developmentally programmed alternative splicing. Differentiation 74 (2-3), 65–80.
- Passmore, L.A., Coller, J., 2022. Roles of mRNA poly(A) tails in regulation of eukaryotic gene expression. Nat. Rev. Mol. Cell Biol. 23 (2), 93–106.
- Pauker, M.H., et al., 2011. Functional cooperation between the proteins Nck and ADAP is fundamental for actin reorganization. Mol. Cell. Biol. 31 (13), 2653–2666.
- Paul, S., et al., 2024. Cerebellar Micro-RNA Profile in a Mouse Model of Spinocerebellar Ataxia Type 2. Neurol. Genet. 10 (2), e200144.
- Pirinen, E., Lo Sasso, G., Auwerx, J., 2012. Mitochondrial sirtuins and metabolic homeostasis. Best Pract. Res. Clin. Endocrinol. Metab. 26 (6), 759–770.
- Prentzell, M.T., et al., 2021. G3BPs tether the TSC complex to lysosomes and suppress mTORC1 signaling. Cell 184 (3), 655–674 e27.
- Prouteau, M., Loewith, R., 2019. TOR signaling is going through a Phase. Cell Metab. 29 (5), 1019–1021.
- Pulst, S.M., et al., 1996. Moderate expansion of a normally biallelic trinucleotide repeat in spinocerebellar ataxia type 2. Nat. Genet. 14 (3), 269–276.
- Ralser, M., et al., 2005a. An integrative approach to gain insights into the cellular function of human Ataxin-2. J. Mol. Biol. 346 (1), 203–214.
- Ralser, M., et al., 2005b. Ataxin-2 and huntingtin interact with endophilin-A complexes to function in plastin-associated pathways. Hum. Mol. Genet. 14 (19), 2893–2909.
- Ramos, R.L., et al., 2024. Patient-specific mutation of Dync1h1 in mice causes brain and behavioral deficits. Neurobiol. Dis. 199, 106594.
- Rehage, N., et al., 2018. Binding of NUFIP2 to Roquin promotes recognition and regulation of ICOS mRNA. Nat. Commun. 9 (1), 299.
- Revach, O.Y., et al., 2015. Mechanical interplay between invadopodia and the nucleus in cultured cancer cells. Sci. Rep. 5, 9466.
- Riggs, C.L., et al., 2020. Mammalian stress granules and P bodies at a glance. J. Cell Sci. 133 (16).

- Robic, A., Demars, J., Kuhn, C., 2020. In-depth analysis reveals production of circular RNAs from non-coding sequences. Cells 9 (8).
- Robic, A., et al., 2022. From the comparative study of a circRNA originating from an mammalian ATXN2L intron to understanding the genesis of intron lariat-derived circRNAs. Biochim. Biophys. Acta Gene. Regul. Mech. 1865 (4), 194815.
- Rodriguez-Silvestre, P., et al., 2023. Perforin-2 is a pore-forming effector of endocytic escape in cross-presenting dendritic cells. Science 380 (6651), 1258–1265.
- Rodriguez-Tornos, F.M., et al., 2016. Cux1 enables interhemispheric connections of layer II/III neurons by regulating Kv1-dependent firing. Neuron 89 (3), 494–506.
- Ross, O.A., et al., 2011. Ataxin-2 repeat-length variation and neurodegeneration. Hum. Mol. Genet. 20 (16), 3207–3212.
- Roundtree, I.A., et al., 2017. Dynamic RNA modifications in gene expression regulation. Cell 169 (7), 1187–1200.
- Roux, K.J., et al., 2009. Nesprin 4 is an outer nuclear membrane protein that can induce kinesin-mediated cell polarization. Proc. Natl. Acad. Sci. USA 106 (7), 2194–2199.
- Rub, U., et al., 2013. Clinical features, neurogenetics and neuropathology of the polyglutamine spinocerebellar ataxias type 1, 2, 3, 6 and 7. Prog. Neurobiol. 104, 38-66
- Ruiz-Gonzalez, Y., et al., 2020. EMG rectification is detrimental for identifying abnormalities in corticomuscular and intermuscular coherence in spinocerebellar ataxia type 2. Cerebellum 19 (5), 665–671.
- Sack, M.N., Finkel, T., 2012. Mitochondrial metabolism, sirtuins, and aging. Cold Spring Harb. Perspect. Biol. 4 (12).
- Sahoo, P.K., et al., 2018. Axonal mRNA transport and translation at a glance. J. Cell Sci. 131 (8).
- Salvi, J.S., et al., 2014. Roles for Pbp1 and caloric restriction in genome and lifespan maintenance via suppression of RNA-DNA hybrids. Dev. Cell 30 (2), 177–191.
- Sanpei, K., et al., 1996. Identification of the spinocerebellar ataxia type 2 gene using a direct identification of repeat expansion and cloning technique, DIRECT. Nat. Genet. 14 (3), 277–284.
- Satterfield, T.F., Pallanck, L.J., 2006. Ataxin-2 and its Drosophila homolog, ATX2, physically assemble with polyribosomes. Hum. Mol. Genet. 15 (16), 2523–2532.
- Satterfield, T.F., Jackson, S.M., Pallanck, L.J., 2002. A Drosophila homolog of the polyglutamine disease gene SCA2 is a dosage-sensitive regulator of actin filament formation. Genetics 162 (4), 1687–1702.
- Schneider, M., et al., 2011. Molecular mechanisms of centrosome and cytoskeleton anchorage at the nuclear envelope. Cell. Mol. Life Sci. 68 (9), 1593–1610.
- Schnetler, R., et al., 2020. Linker histone H1.2 directly activates BAK through the K/RVVKP Motif on the C-Terminal domain. Biochemistry 59 (36), 3332–3346.
- Schols, L., et al., 2015. No parkinsonism in SCA2 and SCA3 despite severe neurodegeneration of the dopaminergic substantia nigra. Brain 138 (Pt 11), 3316–3326.
- Scoles, D.R., Pulst, S.M., 2018. Oligonucleotide therapeutics in neurodegenerative diseases. RNA Biol. 15 (6), 707–714.
- Scoles, D.R., et al., 2017. Antisense oligonucleotide therapy for spinocerebellar ataxia type 2. Nature 544 (7650), 362–366.
- Scoles, D.R., et al., 2022. A quantitative high-throughput screen identifies compounds that lower expression of the SCA2-and ALS-associated gene ATXN2. J. Biol. Chem. 298 (8), 102228.
- Sechi, S., et al., 2021. Identification of GOLPH3 Partners in Drosophila Unveils Potential Novel Roles in Tumorigenesis and Neural Disorders. Cells 10 (9).
- Seidel, G., et al., 2017a. Quantitative global proteomics of yeast PBP1 deletion mutants and their stress responses identifies glucose metabolism, mitochondrial, and stress granule changes. J. Proteome Res. 16 (2), 504–515.
- Seidel, K., et al., 2017b. On the distribution of intranuclear and cytoplasmic aggregates in the brainstem of patients with spinocerebellar ataxia type 2 and 3. Brain Pathol. 27 (3), 345–355.
- Semrad, K., 2011. Proteins with RNA chaperone activity: a world of diverse proteins with a common task-impediment of RNA misfolding. Biochem. Res. Int. 2011, 532908.
- Sen, N.E., et al., 2016. Search for SCA2 blood RNA biomarkers highlights Ataxin-2 as strong modifier of the mitochondrial factor PINK1 levels. Neurobiol. Dis. 96, 115–126.
- Sen, N.E., et al., 2019a. In human and mouse spino-cerebellar tissue, Ataxin-2 expansion affects ceramide-sphingomyelin metabolism. Int. J. Mol. Sci. 20 (23).
- Sen, N.E., et al., 2019b. Generation of an Atxn2-CAG100 knock-in mouse reveals N-acetylaspartate production deficit due to early Nat8l dysregulation. Neurobiol. Dis. 132, 104559.
- Sephton, C.F., et al., 2010. TDP-43 is a developmentally regulated protein essential for early embryonic development. J. Biol. Chem. 285 (9), 6826–6834.
- Shamseldin, H.E., et al., 2020. An exome-first approach to aid in the diagnosis of primary ciliary dyskinesia. Hum. Genet. 139 (10), 1273–1283.
- Shin, E., et al., 2013. Doublecortin-like kinase enhances dendritic remodelling and negatively regulates synapse maturation. Nat. Commun. 4, 1440.
- Singh, R.N., et al., 2017. Diverse role of survival motor neuron protein. Biochim. Biophys. Acta Gene. Regul. Mech. 1860 (3), 299–315.
- Singh, A., et al., 2021. Antagonistic roles for Ataxin-2 structured and disordered domains in RNP condensation. Elife 10.
- Spinelli, R., et al., 2022. ZMAT3 hypomethylation contributes to early senescence of preadipocytes from healthy first-degree relatives of type 2 diabetics. Aging Cell 21 (3), e13557.
- Stubenvoll, M.D., et al., 2016a. ATX-2, the C. elegans Ortholog of Human Ataxin-2, Regulates Centrosome Size and Microtubule Dynamics. PLoS Genet. 12 (9), e1006370.
- Stubenvoll, M.D., et al., 2016b. Correction: ATX-2, The C. elegans Ortholog of Human Ataxin-2, Regulates Centrosome Size and Microtubule Dynamics. PLoS Genet. 12 (12), e1006519.

- Sudhakaran, I.P., et al., 2014. FMRP and Ataxin-2 function together in long-term olfactory habituation and neuronal translational control. Proc. Natl. Acad. Sci. USA 111 (1), E99–E108.
- Swisher, K.D., Parker, R., 2010. Localization to, and effects of Pbp1, Pbp4, Lsm12, Dhh1, and Pab1 on stress granules in Saccharomyces cerevisiae. PLoS One 5 (4), e10006.
- Synofzik, M., et al., 2016. SYNE1 ataxia is a common recessive ataxia with major non-cerebellar features: a large multi-centre study. Brain 139 (Pt 5), 1378–1393.
- Taha, M.S., et al., 2021. Novel FMRP interaction networks linked to cellular stress. FEBS J. 288 (3), 837–860.
- Takakura, Y., et al., 2024. Mitochondrial protein C15ORF48 is a stress-independent inducer of autophagy that regulates oxidative stress and autoimmunity. Nat. Commun. 15 (1), 953.
- Taliaferro, J.M., et al., 2016. Distal alternative last exons localize mRNAs to neural projections. Mol. Cell 61 (6), 821–833.
- Tang, C.X., et al., 2019. Golgin-160 and GMAP210 play an important role in U251 cells migration and invasion initiated by GDNF. PLoS One 14 (1), e0211501.
- Tang, J., et al., 2024. YBX1 underwent phase separation into stress granules stimulated by ionizing radiation. Radiat. Res. 201 (3), 215–223.
- Taylor, J.P., Brown Jr., R.H., Cleveland, D.W., 2016. Decoding ALS: from genes to mechanism. Nature 539 (7628), 197–206.
- Trottier, Y., et al., 1995. Polyglutamine expansion as a pathological epitope in Huntington's disease and four dominant cerebellar ataxias. Nature 378 (6555), 403-406
- van Blitterswijk, M., et al., 2014. Ataxin-2 as potential disease modifier in C9ORF72 expansion carriers. Neurobiol. Aging 35 (10), 2421 e13-7.
- van de Loo, S., et al., 2009. Ataxin-2 associates with rough endoplasmic reticulum. Exp. Neurol. 215 (1), 110–118.
- van den Heuvel, D.M., et al., 2014. Taking a risk: a therapeutic focus on Ataxin-2 in amyotrophic lateral sclerosis? Trends Mol. Med. 20 (1), 25–35.
- Van Langenhove, T., et al., 2012. Ataxin-2 polyQ expansions in FTLD-ALS spectrum disorders in Flanders-Belgian cohorts. Neurobiol. Aging 33 (5), 1004 e17-20.
- Veeraraghavan, P., et al., 2024. Dynamic subtype- and context-specific subcellular RNA regulation in growth cones of developing neurons of the cerebral cortex. bioRxiv. Jan 23:2023.09.24.559186.
- Velazquez-Perez, L., et al., 2016. Abnormal corticospinal tract function and motor cortex excitability in non-ataxic SCA2 mutation carriers: a TMS study. Clin. Neurophysiol. 127 (8), 2713–2719.
- Velazquez-Perez, L., et al., 2017a. Corticomuscular coherence: a novel tool to assess the pyramidal tract dysfunction in spinocerebellar ataxia type 2. Cerebellum 16 (2), 602–606.
- Velazquez-Perez, L., et al., 2017b. Early corticospinal tract damage in prodromal SCA2 revealed by EEG-EMG and EMG-EMG coherence. Clin. Neurophysiol. 128 (12), 2493–2502.
- Velazquez-Perez, L., et al., 2018. Progression of corticospinal tract dysfunction in preataxic spinocerebellar ataxia type 2: a two-years follow-up TMS study. Clin. Neurophysiol. 129 (5), 895–900.
- Vergarajauregui, S., et al., 2020. AKAP6 orchestrates the nuclear envelope microtubuleorganizing center by linking golgi and nucleus via AKAP9. Elife 9.
- Vianna, M.C., et al., 2016. Drosophila Ataxin-2 gene encodes two differentially expressed isoforms and its function in larval fat body is crucial for development of peripheral tissues. FEBS Open Bio. 6 (11), 1040–1053.
- Vilborg, A., et al., 2011. The p53 target Wig-1: a regulator of mRNA stability and stem cell fate? Cell Death Differ. 18 (9), 1434–1440.
- Wang, J.Y., et al., 2015. Sun1 deficiency leads to cerebellar ataxia in mice. Dis. Model. Mech. 8 (8), 957–967.
- Wang, J.Y., et al., 2024. PolyQ-expanded Ataxin-2 aggregation impairs cellular processing-body homeostasis via sequestering the RNA helicase DDX6. J. Biol. Chem. 300, 107413.
- Weiss, L.A., Nieto, M., 2019. The crux of Cux genes in neuronal function and plasticity. Brain Res. 1705, 32–42.
- Woroniuk, A., et al., 2018. STEF/TIAM2-mediated Rac1 activity at the nuclear envelope regulates the perinuclear actin cap. Nat. Commun. 9 (1), 2124.
- Woychek, A., Jones, J.C.R., 2019. Nesprin-2G knockout fibroblasts exhibit reduced migration, changes in focal adhesion composition, and reduced ability to generate traction forces. Cytoskeleton (Hoboken) 76 (2), 200–208.
- Wu, Q.W., Kapfhammer, J.P., 2022. The emerging key role of the mGluR1-PKCgamma signaling pathway in the pathogenesis of spinocerebellar ataxias: a neurodevelopmental viewpoint. Int. J. Mol. Sci. 23 (16).
- Wu, Y.K., et al., 2018. Nesprins and opposing microtubule motors generate a point force that drives directional nuclear motion in migrating neurons. Development 145 (5).
- Xiong, M., et al., 2024. The epithelial C15ORF48/miR-147-NDUFA4 axis is an essential regulator of gut inflammation, energy metabolism, and the microbiome. Proc. Natl. Acad. Sci. USA 121 (27), e2315944121.
- Yamashita, N., Goshima, Y., 2012. Collapsin response mediator proteins regulate neuronal development and plasticity by switching their phosphorylation status. Mol. Neurobiol. 45 (2), 234–246.
- Yang, Y.S., et al., 2019. Yeast Ataxin-2 forms an intracellular condensate required for the inhibition of TORC1 signaling during respiratory growth. Cell 177 (3), 697–710 e17.
- Yao, J., et al., 2021. Nuclear import receptors and hnRNPK mediates nuclear import and stress granule localization of SIRLOIN. Cell. Mol. Life Sci. 78 (23), 7617–7633.
- Yarosh, C.A., et al., 2015. TRAP150 interacts with the RNA-binding domain of PSF and antagonizes splicing of numerous PSF-target genes in T cells. Nucleic Acids Res. 43 (18), 9006–9016.
- Yi, J., et al., 2023. Role of Nesprin-2 and RanBP2 in BICD2-associated brain developmental disorders. PLoS Genet. 19 (3), e1010642.

- Yokoshi, M., et al., 2014. Direct binding of Ataxin-2 to distinct elements in 3' UTRs promotes mRNA stability and protein expression. Mol. Cell 55 (2), 186–198.
- Youn, J.Y., et al., 2018. High-density proximity mapping reveals the subcellular organization of mRNA-associated granules and bodies. Mol. Cell 69 (3), 517–532 e11
- Youn, J.Y., et al., 2019. Properties of Stress Granule and P-Body Proteomes. Mol. Cell 76 (2), 286–294.
- Young, N., et al., 2021. Biallelic SYNE2 missense mutations leading to Nesprin-2 giant hypo-expression are associated with intellectual disability and Autism. Genes (Basel) 12 (9).
- Yu, Z., et al., 2011. PolyQ repeat expansions in ATXN2 associated with ALS are CAA interrupted repeats. PLoS One 6 (3), e17951.
- Yu, X., et al., 2022. Cryo-EM structures of perforin-2 in isolation and assembled on a membrane suggest a mechanism for pore formation. EMBO J. 41 (23), e111857.
- Zappa, F., et al., 2019. The TRAPP complex mediates secretion arrest induced by stress granule assembly. EMBO J. 38 (19), e101704.

- Zhang, X., et al., 2009. SUN1/2 and Syne/Nesprin-1/2 complexes connect centrosome to the nucleus during neurogenesis and neuronal migration in mice. Neuron 64 (2), 173–187.
- Zheng, Y., et al., 2020. A perinuclear microtubule-organizing centre controls nuclear positioning and basement membrane secretion. Nat. Cell Biol. 22 (3), 297–309.
- Zhou, C., et al., 2024. Nesprin-2 coordinates opposing microtubule motors during nuclear migration in neurons. J. Cell Biol. 223 (11).
- Zhuang, Y., et al., 2023. Circadian clocks are modulated by compartmentalized oscillating translation. Cell 186 (15), 3245–3260 e23.
- Zivraj, K.H., et al., 2013. The RNA-binding protein MARTA2 regulates dendritic targeting of MAP2 mRNAs in rat neurons. J. Neurochem. 124 (5), 670–684.
- Zoudilova, M., et al., 2010. beta-Arrestins scaffold cofilin with chronophin to direct localized actin filament severing and membrane protrusions downstream of protease-activated receptor-2. J. Biol. Chem. 285 (19), 14318–14329.